



Measurement Report: Bio-physicochemistry of tropical clouds at Maïdo (Réunion Island, Indian Ocean): overview of results from the BIO-MAÏDO campaign

Maud Leriche^{1,2}, Pierre Tulet³, Laurent Deguillaume^{1,4}, Frédéric Burnet⁵, Aurélie Colomb¹, Agnès Borbon¹, Corinne Jambert³, Valentin DufLOT⁶, Stéphan Houdier⁷, Jean-Luc Jaffrezo⁷, Mickaël Vaïtilingom⁸, Pamela Dominutti^{1,7}, Manon Rocco^{1,#}, Camille Mouchel-Vallon³, Samira El Gdachi^{3,6}, Maxence Brissy^{1,9}, Maroua Fathalli⁵, Nicolas Maury⁵, Bert Verreyken^{10,11,6,*}, Crist Amelync^{10,11}, Niels Schoon¹⁰, Valérie Gros¹², Jean-Marc Pichon⁴, Mickael Ribeiro¹, Eric Pique³, Emmanuel Leclerc³, Thierry Bourriane⁵, Axel Roy⁵, Eric Moulin⁵, Joël Barrie⁵, Jean-Marc Metzger¹³, Guillaume Péris¹⁴, Christian Guadagno¹⁴, Chatrapatty Bhugwant¹⁴, Jean-Mathieu Tibere¹⁴, Arnaud Tournigand¹⁴, Evelyn Freney¹, Karine Sellegri¹, Anne-Marie Delort⁹, Pierre Amato⁹, Muriel Joly⁹, Jean-Luc Baray^{1,4}, Pascal Renard¹, Angelica Bianco¹, Anne Réchou⁶, Guillaume Payen¹³

¹Laboratoire de Météorologie Physique (LaMP), UMR 6016, CNRS, Université Clermont Auvergne, Aubière, 63178, France

²Centre pour l'étude et la simulation du climat à l'échelle régionale, Département des sciences de la terre et de l'atmosphère (ESCER), Université du Québec à Montréal, Montréal, H2X 3Y7, Canada

³Laboratoire d'Aérodynamique (LAERO), UMR 5560, CNRS, Université Paul Sabatier, IRD, Toulouse, 31400, France

⁴Observatoire de Physique du Globe de Clermont-Ferrand (OPGC), UAR 833, CNRS, Université Clermont Auvergne, Aubière, 63178, France

⁵Centre National de Recherches Météorologiques (CNRM), UMR 3589, CNRS, Université de Toulouse, Météo-France, Toulouse, 31057, France

⁶Laboratoire de l'Atmosphère et des Cyclones (LACy), UMR 8105, CNRS, Université de la Réunion, Météo-France, Saint-Denis de la Réunion, 97744, France

⁷Institut des Géosciences de l'Environnement (IGE), UMR 5001, CNRS, IRD, Université Grenoble Alpes, Grenoble, 38000, France

⁸Laboratoire de Recherche en Géosciences et Énergies (LaRGE), EA 4539, Université des Antilles, Pointe-à-Pitre, 97110, France

⁹Institut de Chimie de Clermont-Ferrand (ICCF), UMR 6296, CNRS, Université Clermont Auvergne, Aubière, 63178, France

¹⁰Royal Belgian Institute for Space Aeronomy (BIRA-IASB), Brussels, B-1180, Belgium

¹¹Department of Chemistry, Ghent University, Ghent, B-9000, Belgium

¹²Laboratoire des Sciences du Climat et de l'Environnement (LSCE), UMR 8212, CNRS, CEA, Université Versailles Saint Quentin, Gif-sur-Yvette, 91198, France

¹³Observatoire des Sciences de l'Univers de La Réunion (OSUR), UAR 3365, Saint-Denis de la Réunion, 97744, France

¹⁴ATMO-Réunion, Sainte-Marie, 97438, France

*Now at the Royal Belgian Institute for Space Aeronomy (BIRA-IASB), Brussels, B-1180, Belgium, and at Gembloux Agro-Biotech, University of Liège, Gembloux, B-5030, Belgium

#Now at Instituto de astronomia, geofísica e ciências atmosféricas (IAG), Universidade de São Paulo (USP), Rua do Matão, 1226, Butantã, São Paulo, SP – 05508-090, Brazil

Correspondence to: Maud Leriche (m.leriche@opgc.fr) and Pierre Tulet (pierre.tulet@aero.obs-mip.fr)



Abstract.

The BIO-MAÏDO (Bio-physicochemistry of tropical clouds at Maïdo (Réunion Island): processes and impacts on secondary organic aerosols formation) campaign was conducted from the 13th of March to the 4th of April 2019 on the tropical Réunion Island and implied several scientific teams and state-of-the-art instrumentation. The campaign was part of the BIO-MAÏDO project with the main objective is to improve our understanding of cloud impacts on the formation of secondary organic aerosols (SOA) from biogenic volatile organic compounds (BVOC) precursors in a tropical environment. Instruments were deployed at five sites: a receptor site, the Maïdo observatory (MO) at 2165 m asl, and four sites along the slope of the Maïdo mountain. The obtained dataset includes measurements of the gas-phase mixing ratio of volatile organic compounds (VOC), the characterization of the physical, chemical, and biological (bacterial diversity) properties of aerosols and the characterization of the physical, chemical and biological (identification of viable bacteria through culture-based approaches) properties of the cloud water. In addition, the turbulent parameters of the boundary layer, radiative fluxes, and emissions fluxes of BVOC from the surrounding vegetation were measured to help with the interpretation of the observed chemical concentrations in the different phases. Dynamical analyses show two preferred trajectories routes for air masses arriving at MO during the daytime both corresponding to the return branches of the trade winds associated with the up-slopes thermal breezes. These air masses likely encountered cloud processing during transport along the slope. The highest mixing ratio of oxygenated VOC (OVOC) were measured above the site located in the endemic forest and the highest contribution of OVOC to total VOC at MO. Chemical composition of particles during the daytime shows a higher concentration of oxalic acid and a more oxidized organic aerosol at MO than at other sites along the slope. This is a signature of photochemical aerosols aging along the slope potentially influenced by cloud processing. Despite an in-depth analysis of organic compounds in cloud water, around 80% on average of dissolved organic compounds is undefined highlighting the complexity of the cloud organic matter.

1. Introduction

Aerosols are essential components in the atmosphere as a result of their role in the radiative budget of the earth, including their indirect impact by acting as cloud condensation nuclei (CCN) and ice nuclei (IN) in the formation of cloud droplets and ice crystals. Their impact on climate is still uncertain (Boucher et al., 2013). Aerosols are also a major contributor to air pollution and their health effects have been demonstrated (World Health Organization, 2021). However, there are still major uncertainties in the formation and transformation of atmospheric aerosols. These uncertainties need to be lifted to understand the impacts of these particles on air quality, health, and climate change. Atmospheric aerosols have a complex chemical composition and the organic fraction, which contributes significantly to the total mass of fine particles (Jimenez et al., 2009), is still the least characterized to date. 3D atmospheric chemistry models are globally unable to reproduce the observed amount, oxidation level, and spatial distribution of organic aerosols (Heald et al., 2011; Jathar et al., 2016; Pai et al., 2020). Among this organic fraction, a major part of the mass is of secondary origin (Zhang et al., 2007). The main precursors of the secondary organic aerosols (SOA) are natural compounds (isoprene and terpenes) and aromatics from anthropogenic origin. Even if the



chemical reactivity in the gaseous phase of these volatile organic compounds (VOC) is relatively well known, the nature and the potential of SOA formation of their oxidation products are still uncertain. Biogenic VOC (BVOC) from terrestrial
75 vegetations are particularly important since they dominate the global emission of nonmethane hydrocarbons in the atmosphere (Guenther et al., 2012). The oxidation of BVOC in the atmosphere forms less volatile oxidized chemical species, which participate in SOA formation through various complex processes (Shrivastava et al., 2017). These oxidized products are soluble in water where they are photo-oxidized (Ervens et al., 2011). The chemical reactivity in aqueous phase is different than in the gas phase and can lead to the formation of low volatility compounds (Carlton et al., 2007; Liu et al., 2009) including
80 oligomers (Renard et al., 2015). It is now well established that the aqueous phase oxidation contribution to the SOA formation is significant (McNeil, 2015; Su et al., 2020 in polluted conditions) but still misunderstood in term of processes and badly represented in 3D models (Ervens, 2015). The main contributors to SOA formation from cloud chemistry are known to be low volatility organic acids coming mainly from the photo-oxidation of glyoxal and methylglyoxal (Ervens et al., 2011). Recently, Tsui et al. (2019) showed that isoprene epoxydiols (IEPOX) could be a significant contributor to SOA formation from cloud
85 chemistry. The presence of bacteria in cloud water also has a potential impact on cloud chemical composition (Vaätilingom et al., 2013; Khaled et al., 2021). A recent study on at the global scale estimates that microbial processes might lead to a loss of water-soluble organic content in cloud droplets of the same order of magnitude than the loss from chemical processes (Ervens and Amato, 2020). However, this estimation is very uncertain, and, to the best of our knowledge, no study has assessed the effect of microbial processes in cloud droplets on SOA formation.

90 Humid tropical atmospheres, which are characterized by high biogenic emissions and a high occurrence of fogs and clouds, is particularly favorable to SOA formation through biogenic precursors via cloud multiphase chemistry. Réunion Island is a small tropical island in the Indian Ocean at the east of Madagascar Island. Anthropogenic sources are limited in the island and are mainly in the coastline area, as the island is far from the impact of large anthropogenic emission sources (Dufлот et al., 2019). La Réunion is a volcanic island with an abrupt topography and high mountainous area (Piton des Neiges, 3070 m) and presents
95 100 000 ha of native ecosystems (Dufлот et al., 2019). Lesouëf et al. (2011; 2013) described the complex atmospheric dynamic on the island, which is, at the large scale, affected by easterly/south-easterly trade winds near the ground and westerlies in the free troposphere. Due to the strengthening of the large-scale subtropical subsidence at night, air masses at high altitude are disconnected from local and regional anthropogenic sources during the night and early morning.

The Maïdo atmospheric observatory (altitude 2165 m) (Baray et al., 2013), close to the Piton Maïdo (2190 m), is in the
100 northwest part of the island and offers a unique opportunity to study SOA formation processes in the humid tropical atmosphere. The slope of the Maïdo, west of the observatory, is covered with tropical forests characterized by endemic tree species *Acacia heterophylla* (*Fabaceae*), plantations of the coniferous species *Cryptomeria japonica* (*Taxodiaceae*) and the *Acacia heterophylla* forest, locally called “Tamarinaie” (Dufлот et al., 2019). A first campaign devoted to cloud-aerosols interaction (Dufлот et al., 2019) in March-April 2015 showed the potential of the observatory to study the formation of SOA
105 influenced by clouds with the diurnal formation of clouds on the slope below the observatory over Tamarinaie, which emits



isoprene and terpenes, and their dissipation at the level of the observatory. Measurements performed during this campaign showed high levels of formaldehyde, a product of isoprene oxidation and the presence of viable bacteria in cloud water.

The BIO-MAÏDO (Bio-physicochemistry of tropical clouds at Maïdo (Réunion Island): processes and impacts on secondary organic aerosols formation) project was designed in this context with three main objectives: (i) to understand which are the main formation pathways of SOA in humid tropical atmosphere (gaseous phase versus aqueous phase); (ii) to improve multiphase processes leading to SOA formation in 3D model; (iii) to examine whether the presence of bacteria in aqueous phase could contribute to SOA formation. The strategy of BIO-MAÏDO is based on an intensive field campaign using the Maïdo observatory facilities, in synergy with modelling studies using: two lagrangian particle dispersion models FLEXPART-AROME (Verreyken et al., 2019) and Meso-CAT (Rocco et al., 2022), a 0D cloud chemistry model (CLEPS, Mouchel-Vallon et al., 2017; Rose et al., 2018) and a 3D model coupling meteorology and chemistry and including a cloud chemistry module (Meso-NH, Lac et al., 2018; <http://mesonh.aero.obs-mip.fr/>, last access: 20 June 2023).

The aim of the present paper is to present an overview of the results obtained from the campaign. The general strategy of the campaign and the description of the five sampling sites are provided. Then, main results obtained from measurements are summarized describing the boundary layer evolution and cloud cycles, gas, aerosol and cloud chemistry.

120 2. Strategy of the campaign and sites description

2.1 Strategy

In the general context of the three main objectives of the BIO-MÄIDO project presented above, the field campaign aims to: (1) characterize the chemical and biological composition of air and cloud samples and identify main sources of gases and aerosols; (2) characterize the dynamics and the evolution of the boundary layer and the macro and micro-physical properties of clouds; (3) determine case studies for modelling work with CLEPS and Meso-NH.

The campaign took place from the 13th of March to the 4th of April 2019. This period was chosen to include frequent periods of formation of low-level cloud and of convective precipitating clouds along the slopes of the Maïdo (Duflot et al., 2019), a high UV index (12) and high temperatures (end of the southern summer). Moreover, the campaign took place during the 2-years observation period of the OCTAVE project (Oxygenated Compounds in the Tropical Atmosphere: Variability and Exchanges, <http://octave.aeronomie.be>, last access: 20 June 2023) during which complementary instrumentations were deployed at the Maïdo observatory to characterize oxygenated volatile organic compounds (OVOC) mixing ratios. The main objective of OCTAVE is to improve the climatology of the global budget of OVOC and their role in tropical regions (Rocco et al., 2020; Simu et al., 2021; Verreyken et al., 2021).

The field campaign included five sampling sites (Figure 1). Except for the Maïdo observatory, these sites are all located along the northwestern slope to the Maïdo site, identified as one of the two main paths for dominant winds. At the mid-morning almost every day, clouds form on the slope of the Maïdo, and in general evaporate at the altitude of the observatory (Duflot et al., 2019).



An innovative instrumentation was deployed, including for instance: three proton-transfer-reaction mass spectrometer (PTR-MS) for online analysis of VOC, one of which was operated at high frequency and coupled to an ultrasonic anemometer allowed measurements of BVOC fluxes; a tethered balloon to capture microphysical characteristics of clouds; an aerosol chemical speciation monitor (ACSM), which provides online measurements of the non-refractory submicron chemical composition (NR-PM₁); a new generation of cloud droplet impactor to accumulate cloud water and allow biological (bacteria diversity and number concentration, ATP quantification) and detailed chemical analyses further in the lab. For instance, dissolved organic compounds have been intensively investigated in cloud water to characterize their atmospheric sources, evaluate the chemical and biological processes occurring in the air during the transport of the organic matter, and to assess their partitioning among the gas and aqueous phases.

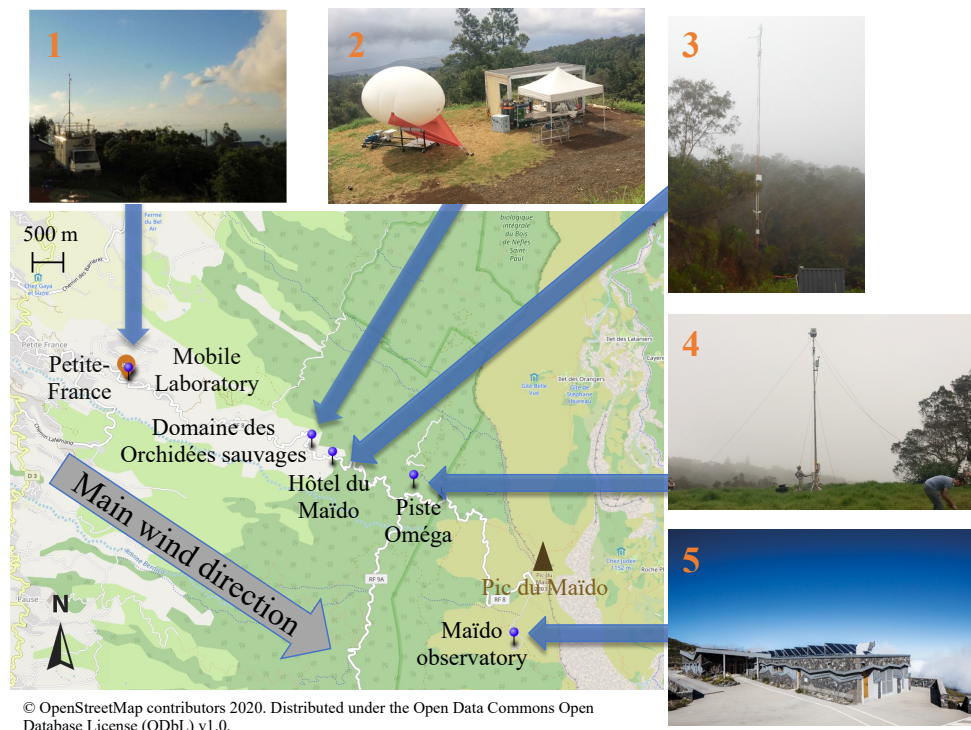


Figure 1. Location of the five-instrumented sites during the BIO-MAÏDO campaign.

During the whole campaign, FLEXPART (Pisso et al., 2019) coupled with the AROME operational forecasts at 2.5 km of horizontal resolution (Verreyken et al., 2019) was used to analyze the regional origin (marine boundary layer, free troposphere) of the air masses observed at the Maïdo area (https://geosur.osureunion.fr/public_html/cgi-bin/web/display_biomaido_v2.py, last access: 20 June 2023). This information has been supplemented by back-trajectories computed with Meso-CAT (Rocco et al., 2022) resulting from the coupling between high-resolution Meso-NH simulations and the lagrangian tool CAT (Computing Advection-interpolation of atmospheric parameters and Trajectory tool; Baray et al., 2020). These back-trajectories allowed



155 assessing the local contribution of biogenic, anthropogenic, and marine source area in the chemical composition of air masses
sampled at the sampling sites and to determine which days present a dynamical connection between the sites.

2.2 Petite France (PF-1): a rural site under urban influence

Petite France (PF-1, 965 m asl, 21°02'33.3"S 55°19'32"E) is a neighborhood/district of the municipality of Saint-Paul. The
land-cover around PF-1 comprises mainly of residential areas, grassland, and sugar cane plantations. A part of the instruments
160 is deployed inside the monitoring truck of Atmo-Réunion (<https://atmo-reunion.net/>, last access: 20 June 2023), the association
in charge of the air quality monitoring on the island. Instrumentation deployed at PF-1 aimed at characterizing the chemical
composition of the air including gases and PM₁₀. The instrumentation onboard the truck included analyzers for ozone, carbon
monoxide, nitrogen oxides, sulfur dioxide, a particle counter for PM_{2.5} and a proton-transfer-reaction quadrupole mass
spectrometer (PTR-QMS) for online VOC characterization. The chemical and biological composition of PM₁₀ was analyzed
165 from pure quartz fiber filters sampled twice a day during night and day with a high-volume sampler. Various chemical analyzes
on filters were performed in the lab to quantify the major chemical constituents and specific chemical tracers. The carbonaceous
fraction of particles (EC and OC) was analyzed with a Sunset Lab analyzer (using the EUSAAR2 thermo-optical protocol,
Cavalli et al., 2010). The major ions components were measured by ion chromatography using an ICS300 Chromatograph
(dual-channel, Thermo-Fisher) following the standard protocol described in Jaffrezo et al. (2005). Anhydro-sugars and
170 saccharides were analyzed by high-performance liquid chromatography with pulsed amperometric detection (HPLC-PAD,
using an ICS 5000+ Chromatograph, Samake et al., 2019). The analysis of organic acids was conducted using a HPLC-MS
(GP40 Dionex), with negative mode electrospray ionization (Borlaza et al., 2021). The diversity of bacteria in PM₁₀ samples
was investigated by high-throughput sequencing (Illumina) of metabarcoded ribosomal gene amplicons, from whole genomic
DNA extracted using the commercial DNeasy PowerWater kit (Qiagen). Polymerase chain reaction (PCR) amplification was
175 performed using the primers 515F and 806R, as recommended by the Earth Microbiome Project (Caporaso et al., 2012). The
sequence data obtained from Illumina MiSeq (2x250bp) were analyzed through the FROGS pipeline (Escudié et al., 2018)
using Silva 132 as the reference database (Quast et al., 2013), as in Péguilhan et al. (2021). In addition, a ceilometer was
deployed to characterize the boundary layer evolution and the cloud cycle. Table 1 summarizes the instruments deployed at
PF-1 and the associated measured parameters.

180



Table 1. Instrumentations deployed at PF-1 and associated measured parameters.

Instrument	Measured parameter	Sampling frequency	Institution in charge
Ultrasonic wind sensor Windsonic , Gill Instruments	Wind	15 min	Atmo-Réunion
Humidity and temperature sensor EE210, E+E Elektronik GmbH	Temperature Relative humidity	15 min	Atmo-Réunion
CO analyzer T300, Teledyne API	Mixing ratio of CO	15 min	Atmo-Réunion
Ozone analyzer O342M, Environnement SA	Mixing ratio of O ₃	15 min	Atmo-Réunion
NO/NO₂/NO_x analyzer T200, Teledyne API	Mixing ratio of NO, NO ₂ , NO _x ,	15 min	Atmo-Réunion
SO₂ analyzer 43i, Thermo Fisher Scientific Inc.	Mixing ratio of SO ₂	15 min	Atmo-Réunion
PTR-QMS, Ionicon Analytik GmbH	Mixing ratio of COV	1 min	LSCE
Aerolaser AL4021, Aero-Laser GmbH	Mixing ratio of HCHO	1 min 28/03-04/04	LaMP
Condensation Particle Counter MAGIC CPC, Aerosol Devices Inc.	Number concentration of particles with diameter from 5 nm to 2.5 μm	10 s	Atmo-Réunion
High Volume Sampler (Hi-VOL) Digital DA80, Megatec – filter	PM ₁₀ mass chemical concentration and bacterial diversity	Day and night 10-12 h	IGE
PQS1 radiometer, Kipp & Zonen	Photosynthetic Active Radiation (PAR)	15 min	CNRM
Ceilometer CT25K, Vaissala	Cloud base height Backscatter profile	1 min 1 min	LACy



2.3 Domaine des Orchidées Sauvages (DOS-2): a strategic site to observe cloud cycle

185 Domaine des Orchidées Sauvages (DOS-2, 1465 m asl, 21°03'07"S 55°21'11"E) is a large private property where the tethered
balloon was operated. Moreover, several sets of devices were also deployed there: a meteorological station, complementary
probes monitoring the size spectrum of particles, a present weather visibility sensor associated with a droplet size spectrometer
to characterize the microphysical properties of clouds, as well as a ceilometer and the Lidar MARLEY (Mobile AeRosol
Raman Lidar for troposphEre surveY) to characterize the boundary layer evolution, the cloud cycle, and the vertical profile of
aerosols. The land cover around DOS-2 is composed mainly of a mix of grassland and forests.

190 The tethered balloon was equipped with an ultrasonic anemometer and a temperature probe at high frequency to estimate the
heat and momentum fluxes and the turbulent kinetic energy by eddy covariance. At the beginning of the morning, the tethered
balloon was operated in clear sky with an aerosol probe whereas it was operated with cloud sensors at the end of the morning
when cloud appeared. The tethered balloon was operated for 21 days for 144 hours of measurements. Following Fathalli et al.
(2022), the adopted strategy was alternating vertical soundings and levels at constant altitude (20 minutes for turbulence, or 5
195 to 10 minutes for cloud microphysics statistical representativeness) for each flight. Table 2 summarizes the instruments
deployed at DOS-2 and the associated measured parameters.



Table 2. Instrumentations deployed at DOS-2 and associated measured parameters.

Instrument	Measured parameter	Sampling frequency	Institution in charge
Condensation Particle Counter CPC3788, TSI	Total number concentration of aerosols with diameter from 2.5 nm to 2.5 μm	1 s	CNRM
Scanning Mobility Particle Sizer SMP3080, TSI	Size spectrum of aerosols with diameter from 10 nm to 500 nm	3 min	CNRM
Optical Particle Sizer OPC3330, TSI	Size spectrum of aerosols with diameter from 0.3 μm to 10 μm	5 min	CNRM
CCNC Droplet Measurement Technologies Fog monitor, Droplet Measurement Technologies	Number concentration of CCN at S = 0.1%, 0.2% and 0.3% supersaturation	5 min for each	CNRM
Present Weather Detector Vaisala	Visibility Rain Luminance	15 s 15 s 15 s	CNRM
Lidar MARLEY	Backscatter profile	1 min	LACy
Ceilometer CS135, Campbell Scientific	Cloud base height Backscatter profile	10 s 10 s	LACy
Tethered Balloon			
Optical particle counter (OPC), MetOne	Size spectrum of aerosols with diameter from 0.5 μm to 10 μm	6 s	CNRM
Cloud drop probe (CDP), Droplet Measurement Technologies	Size spectrum of droplets with diameter from 2 μm to 50 μm	1 s	CNRM
Sonic anemometer	Wind Temperature Relative humidity	20 Hz 20 Hz 20 Hz	CNRM



2.4 Hôtel du Maïdo (HM-3): a forest area dedicated to fluxes measurements

200 Hôtel du Maïdo (HM-3, 1500 m asl, 21°03'16.4"S 55°21'21.4"E) is a former holiday camp located in the middle of the forest. This site was dedicated to measurements of VOC fluxes. A 24 m instrumented mast and a container had been installed on the site. Several devices were deployed on the top of the mast: an ultrasonic anemometer including a temperature probe and an analyzer of carbon dioxide and water vapor. An inlet connected to a pump inside the container had been also installed at the top of the mast. This inlet brought air inside the container to several devices: a second analyzer of carbon dioxide and water
205 vapor, an ozone analyzer, a proton-transfer-reaction time of flight mass spectrometer (PTR-TOFMS) for VOC measurements and an active sampling on sorbent cartridges. The comparison of measurements from both analyzers of carbon dioxide and water vapor allowed estimating the effects of the inlet on other chemical compounds measurements inside the container. Measurements of the mixing ratio of biogenic organic compounds (isoprene and monoterpenes) by PTR-TOFMS at 5 Hz were used to estimate their emissions thanks to the ultrasonic anemometer by eddy covariance. Finally, measurements of shortwave
210 and longwave, upward and downward radiative fluxes, as well as of visibility and photosynthetically active radiation (PAR) were operated at the bottom part of the mast. Table 3 summarizes the instruments deployed at HM-3 and the associated measured parameters.



Table 3. Instrumentations deployed at HM-3 and associated measured parameters.

Instrument	Measured parameter	Sampling frequency	Institution in charge
3D Sonic anemometer CSAT 3, Campbell Scientific	Wind, temperature, relative humidity	10 Hz	LAERO
LI-7500 open path gas analyzer, LI-COR	Mixing ratio of CO ₂ and H ₂ O (mast)	10 Hz	LAERO
CNR4 radiometer, Kipp & Zonen	Up and down, longwave and shortwave radiations	1 min	LAERO
Present Weather Detector PWD22, Vaisala	Visibility	15 s	CNRM
	Rain	15 s	
	Luminance	15 s	
PQS1 radiometer, Kipp & Zonen	Photosynthetic Active Radiation (PAR)	1 min	LAERO
LI-6262 closed path gas analyzer, LI-COR	Mixing ratio of CO ₂ and H ₂ O (container)	10 Hz	LAERO
O₃ analyzer TEI49i, Thermo Fisher Scientific Inc.	Mixing ratio of O ₃	5 min	LAERO
PTR-ToF-MS 1000 ultra, IONICON	Mixing ratio of VOC	5 Hz	LAERO
Smart Automatic Sampling System (SASS)	Mixing ratio of VOC	5 cartridges/day 18/03-05/04	LaMP

215

2.5 Piste Omega (PO-4): a forest site to sample cloud water

Piste Oméga (PO-4, 1760 m asl, 21°03'26.8"S 55°22'05.0"E) is a forest trail from the Maïdo road. The site is surrounded by forest. A 10 m mobile mast was used to install a cloud impactor (cf. Fig. 1). This collector was facing the slope from which the cloud came. A modified cloud drop probe (CDP) had been fixed on the mast just under the cloud collector to monitor the cloud microphysical properties. It measures the droplet size distribution from 2 to 50 µm in diameter, enabling the calculation of the liquid water content (LWC) and of the effective diameter (D_{eff}). A meteorological station had also been fixed on the mast (T, RH, wind speed). Finally, the AEROVOCC sampler has been installed on the side of the cloud collector. AEROVOCC

220



was developed to sample VOC and OVOC in cloudy air. It consists of three sorbent cartridges connected to three automated pumps to control samples at a constant flow.

225 During the whole campaign, 14 cloud water samples have been collected (named from R1 to R14 hereafter). The mean volume of samplers was 111 mL. The sampled cloud water was further analyzed in lab for (1) pH; (2) main inorganic ions by ionic chromatography; (3) total organic carbon (TOC) by TOC analyzer; (4) targeted organic compounds by high-performance liquid chromatography (HPLC) – mass spectrometry (MS) for carboxylic acids, by HPLC with fluorescence detection (HPLC-Fluo) for carbonyl compounds, by HPLC-high resolution mass spectrometry (LC-HRMS) for amino acids, by HPLC with pulsed amperometric detector (HPLC-PAD) for sugars, by stir bar sorptive extraction (SBSE) coupled to gas chromatography-mass spectrometry (GC-MS) for low soluble VOC; (5) hydrogen peroxide by derivatization and spectro-fluorescence and, Fe(II) and Fe(III) by complexation and ultraviolet-visible spectrophotometry (UV/Vis spectrophotometer). When enough volume of water was available, a non-target analysis was performed to investigate the complexity of the dissolved organic matter. 3 clouds were analyzed by Fourier Transform Ion Cyclotron Resonance Mass Spectrometry (FT-ICR MS), using ionization in positive and negative polarity and multiple ionization sources to get a full picture of the composition of organic matter.

230 Viable culturable bacteria were investigated by culture-plating of 0.1 mL of water samples on R2A medium and incubation at 25°C in the dark. Colonies were isolated and taxonomically identified based on full length 16S rRNA gene sequences, obtained from PCR amplification using the primers 27f and 1492r, and online BLAST software available from NCBI’s website, as in Vaithilingom et al., 2012. Table 4 summarizes the instruments deployed at PO-4 and the associated measured parameters.

240

Table 4. Instrumentations deployed at PO-4 and associated measured parameters.

Instrument	Measured parameter	Sampling frequency	Institution in charge
Meteorological station	Wind, temperature Pressure, relative humidity	1 min	CNRM
Cloud drop probe (CDP), Droplet Measurement Technologies	Size spectrum of droplets with diameter from 2 μm to 50 μm	1 s	CNRM
AEROVOCC	Mixing ratio of VOC and OVOC	One sample by event	LaMP
Cloud impactor	Chemical composition of cloud water Viable bacteria diversity	Duration of the event	LaMP



2.6 Maïdo observatory (MO-5): a receptor site to observe process air mass

Maïdo observatory (MO-5, 2165 m asl, 21°04'46"S 55°22'59"E) is surrounded by mountain shrublands. Previous simulations
245 with the 3D Meso-NH model showed the vanishing of clouds at the same period of the year than the campaign at the
observatory altitude (Dufлот et al., 2019).

The Maïdo observatory (Baray et al., 2013) can host atmospheric scientific experiments and offer the possibility for scientists
to stay on site. Several European and international observation services operate at the observatory, and associated routine
observations are done, in particular, of interest for BIO-MAÏDO: for aerosols (submicron size distribution, CCN concentration,
250 and total PM_{2.5} number concentration), for gases (mixing ratio of ozone, nitrogen oxides, carbon monoxide and sulfur dioxide)
and basic meteorological parameters. The BIO-MAÏDO campaign also benefited from the two-year presence (October 2017
to November 2019) at the observatory of the high-sensitivity quadrupole-based PTR-MS of BIRA-IASB as part of the
OCTAVE project. This suite of instruments was complemented by the online chemical characterization of non-refractory PM₁
using the Time-of-Flight Aerosol chemical speciation monitor (ToF-ACSM), PM₁₀ filter sampling using a high-volume
255 sampler identical to those deployed at PF-1 (Dominutti et al. 2022b), and by the same set of instruments deployed at DOS-2
to characterize the microphysical properties of clouds. The chemical and biological analyses of PM₁₀ performed from filters
are the same as at PF-1. The MO-5 station is also part of the ACTRIS (Aerosol, Clouds and Trace Gases Research
Infrastructure) monitoring network and monitors aerosol size distribution and number concentration using a custom-made
differential mobility particle sizer (DMPS) with a commercially available condensation particle counter (CPC, TSI). Table 5
260 summarizes the instruments deployed at MO-5 and the associated measured parameters.



Table 5. Instrumentations deployed at MO-5 and associated measured parameters.

Instrument	Measured parameter	Sampling frequency	Institution in charge
Fourier-transform infrared spectroscope (FTIR)	Wind, temperature Pressure, relative humidity	1 min	OPAR/BIRA-IASB
CO analyzer Horiba	Mixing ratio of CO	1 min	OPAR
O₃ analyzer TEI49i, Thermo Fisher Scientific Inc.	Mixing ratio of O ₃	1 min	OPAR
NO_x analyzer, Environnement SA AC31M	Mixing ratio of NO _x , NO, NO ₂	1 min	OPAR
SO₂ analyzer T421, Thermo Fisher Scientific Inc.	Mixing ratio of SO ₂	1 min	OPAR
Condensation Particle Counter CPC3776, TSI	Number concentration of particles with diameter from 25 nm to 1 μm	10 s	OPAR
Custom-made Differential Mobility Particle Sizer with a Condensation Particle Counter CPC3100, TSI	Size spectrum of aerosols with diameter from 13.7 nm to 650 nm, 14 size classes	8 min	OPAR/LaMP
Aerosol Chemical Speciation Monitor ToF-ACSM, Aerodyne Research Inc.	Chemical composition of NR-PM ₁	10 min	LaMP
High Volume Sampler (Hi-VOL) Digital DA80, Megatec – filter	PM ₁₀ mass chemical concentration and biological composition	Day and night 10-12 h	IGE
PTR-MS, Ionicon Analytik GmbH	Mixing ratio of VOC	2.7 min	BIRA-IASB
Aerolaser AL4021, Aero-Laser GmbH	Mixing ratio of HCHO	1 min 13/03-27/03	LaMP
Fog monitor, Droplet Measurement Technologies	Size spectrum of droplets with diameter from 2 μm to 50 μm	1 s	CNRM
Present Weather Detector PWD22, Vaisala	Visibility Rain Luminance	15 s 15 s 15 s	CNRM



3. Main results

265 A large range of data was collected during the BIO-MAÏDO campaign. The cloud water collector deployed at PO-4 (Dominutti et al., 2022a) allowed more efficient sampling of cloud droplets than during the FARCE campaign (Duflot et al., 2019). Table S1 in the supplement summarizes the daily operation of all instruments deployed during the campaign. This report has been used to identify the days with the maximum amount of information available.

3.1 Meteorological overview of the campaign

270 The meteorological environment of Reunion Island (Réchou et al., 2019), and particularly of the Maïdo area, has been extensively studied in recent years in the frame of many measurement campaigns performed at the Maïdo observatory. Lesouëf et al. (2011), Guilpart et al. (2017) and Foucart et al. (2018) have highlighted the main local and regional circulations that affect measurements at the observatory. Lesouef et al. (2013) and Duflot et al. (2019) studied the evolution of the mixing boundary layer and highlighted the superposition of several stratified layers along the Maïdo slopes. These previous results are summarized below.

275 For the main meteorological circulations that affect the campaign area, Reunion Island is subject to a strong easterly/southeasterly trade wind flow in winter and a weaker one in summer in the lowest layers of the atmosphere when the intertropical convection zone is close to Réunion Island. The Maïdo region located to the northwest of the island is conditioned by the convergence of two distinct flows: (i) The overflow regime due to the lifting of the trade winds over the topography of the island. This flow mainly affects the free troposphere; (ii) The counterflow regime corresponding to the circumvention of the trade winds around the topography. This low and medium altitude flow leads to a return flow generally located in the west and north-west sector, downwind of the island.

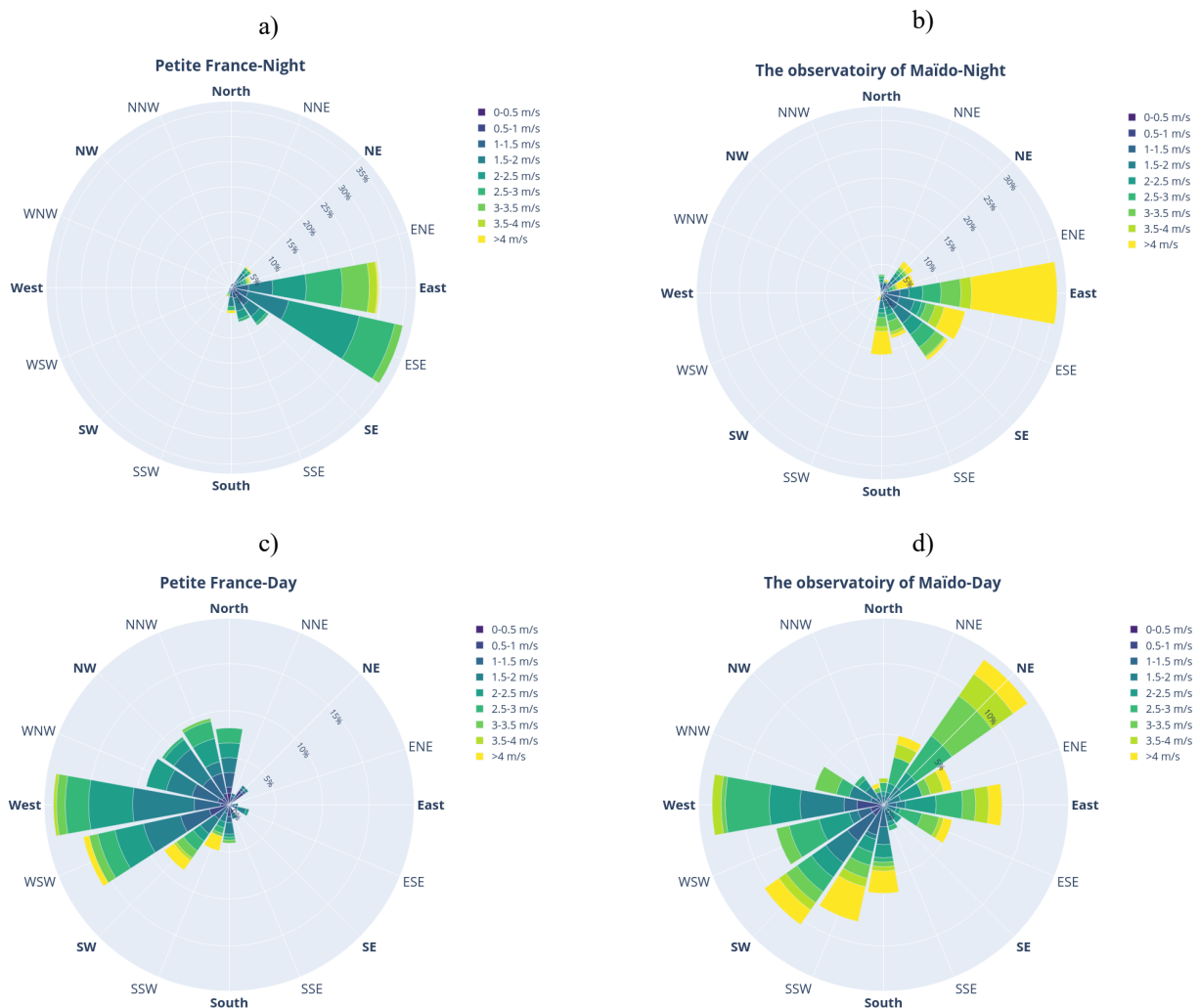
285 More locally, thermal breezes strongly influence the weather during the daytime: near the coast, sea/land breezes are formed and higher up, anabatic/catabatic breezes affect the slopes during the day/night. All these circulations lead to ascents on the slopes of Maïdo almost daily with clouds formation in the middle of the morning and beginning of the afternoon, then subsidence and stratification of the boundary layer leading to the evaporation of the clouds at the end of the daytime. The Maïdo observatory is generally located in the trade winds overflow flow except in the middle of the day when it is located close to a convergence zone between the overflow flow and the thermal ascents on the slopes. At night, the observatory is located in the free troposphere.

290 These different mechanisms have been highlighted mainly by numerical modeling and on case studies lasting a few days. The availability of two meteorological stations located at PF-1 (mid-slope) and MO-5 (summit) during the BIO-MAÏDO campaign, made it possible for the first time to characterize thermal breezes on the Maïdo slope over a period of 27 days corresponding to the transition period between the wet season and the dry season.

The weather conditions observed during the campaign are summarized by the wind roses resulting from local observations in Figure 2. Fig. 2a and 2b correspond to the wind observed at PF-1 and MO-5 between 14 UTC and 04 UTC (i.e. from the end



295 of the afternoon to the beginning of the morning). At both stations, the wind regime is from the south and south-east, with a maximum wind speed between 2 to 3 m s⁻¹ at PF-1 (frequency 35%) and higher than 4 m s⁻¹ at MO-5 (frequency 15%). These conditions show the strong influence of the trade winds and the overflow conditions at night. The wind conditions observed during the daytime (from 04 UTC to 18 UTC; Fig. 2c and 2d) are more variable, especially at MO-5. At PF-1, the flow is essentially from the west (30 %) and of lower intensity than at MO-5 (generally between 1 and 3 m s⁻¹). This direction is
300 typical to the up flow of the air mass on the slopes by thermal breezes or by the return flow of the trade winds. At MO-5, the air masses have two opposite directions: from the north (14%) to the east (8%) and from the south (6 %) to the west (20 %). This indicates a reversal of the wind direction during the daytime, as observed by Rocco et al. (2022). These conditions were consistent with the period of transition from the wet to the dry season.



305 **Figure 2. Wind rose at PF-1 and MO-5 between 14 UTC and 04 UTC (nighttime) and from 04 UTC to 18 UTC (daytime) averaged over the entire campaign from March 11 to April 7. The intensity is in m s⁻¹.**



Verreyken et al. (2020; 2021) and Rocco et al. (2020) studied the origin of the air masses measured at the Maïdo observatory by using Lagrangian trajectory tools (FLEXPART, CAT). Their results concerned the origin of air masses from the atmospheric transport at the synoptic scale and showed that the dominant large-scale air masses are easterly under the influence of trade winds and that the strongest biogenic contributions coincided with air masses passing over the northeastern part of La Réunion. For the BIO-MÃIDO campaign, to determine the origin of the air masses arriving at PF-1 and MO at the scale of the entire island, high spatio-temporal back-trajectories have been calculated using Meso-CAT. The used Meso-NH simulations cover the whole campaign and use three embedded domains at 2 km, 500 m and 100 m of horizontal resolution. Rocco et al. (2022) first exploited these back-trajectories by combining them with soil data from the Corine 2018 land-cover database (Geoportail, <https://www.geoportail.gouv.fr/>, last access: 20 June 2023) to assess the origin of the air masses sampled at MO. Moreover, the dominant circulations schemes at the scale of the highland are better highlighted by new elements provided here and obtained by calculating footprint maps using Meso-CAT in back-trajectory mode.

Figures 3 gives the footprint of PF-1 and MO-5 using back-trajectories of Meso-CAT from the 500 m of horizontal resolution domain. These footprints are computed by assembling all the back-trajectories that reached these two stations and by counting all the trajectory points per pixel of 1 km size. Two types of footprints have been calculated, a first which corresponds to the total atmospheric column, keeping all the trajectory points (Fig. 3a and 3b), and a second for which we select only the trajectory points located less than 500 meters above the ground level and during the mid-day (between 06 UTC to 14UTC; Fig. 3c and 3d).

The total column footprint of PF-1 (Fig. 3a) clearly shows the influence of the trade winds with air masses arriving from the south-east, bypassing the island of La Reunion Island as much from the north as from the south, and arriving on PF-1 generally with an ascent by the slopes. These air masses are well channeled and bypass the topography by the southern flank of Reunion Island. The main part of back-trajectories arrives locally from the west and is more variable and diffuse over the whole campaign period. At MO-5 (Fig 3b), there is a wider dispersion of air mass origins. The signature of the trade winds is even more visible with air masses arriving at MO-5 generally more directly and pass mainly through the south. The footprint also shows more trajectory points east of MO-5, indicating the influence of frequent ascents of air masses from the Cirque de Mafate.

To study the mixing boundary layer air masses advected by thermal breezes, other footprints have been calculated according to the following criteria: (i) only the back-trajectories remaining in the mixing boundary layer arbitrarily set as a 500 m (above ground level) thick layer are kept; (ii) we have retained the periods of the day when there are back-trajectories coming from south-west to north-west, between 06 UTC and 14 UTC (Fig. 3c and 3d). Again, two preferred trajectories routes can be seen for PF-1 and for MO-5, the main part of the air masses passing through the south. This means that the PF-1 measurements were able to load themselves with chemical and biological compounds over the forests located between 1000 m and 1500 m asl in the south-west of the island. The other well-marked result is the one going up the western flank of the island, whose trajectories also show a passage in the marine boundary layer. By differences with the total day integration, one can note that



340 most of the back-trajectories modeled at MO-5 come from the south to the north-west, which corresponds to the return branches of the trade winds associated with the up-slopes thermal breezes.

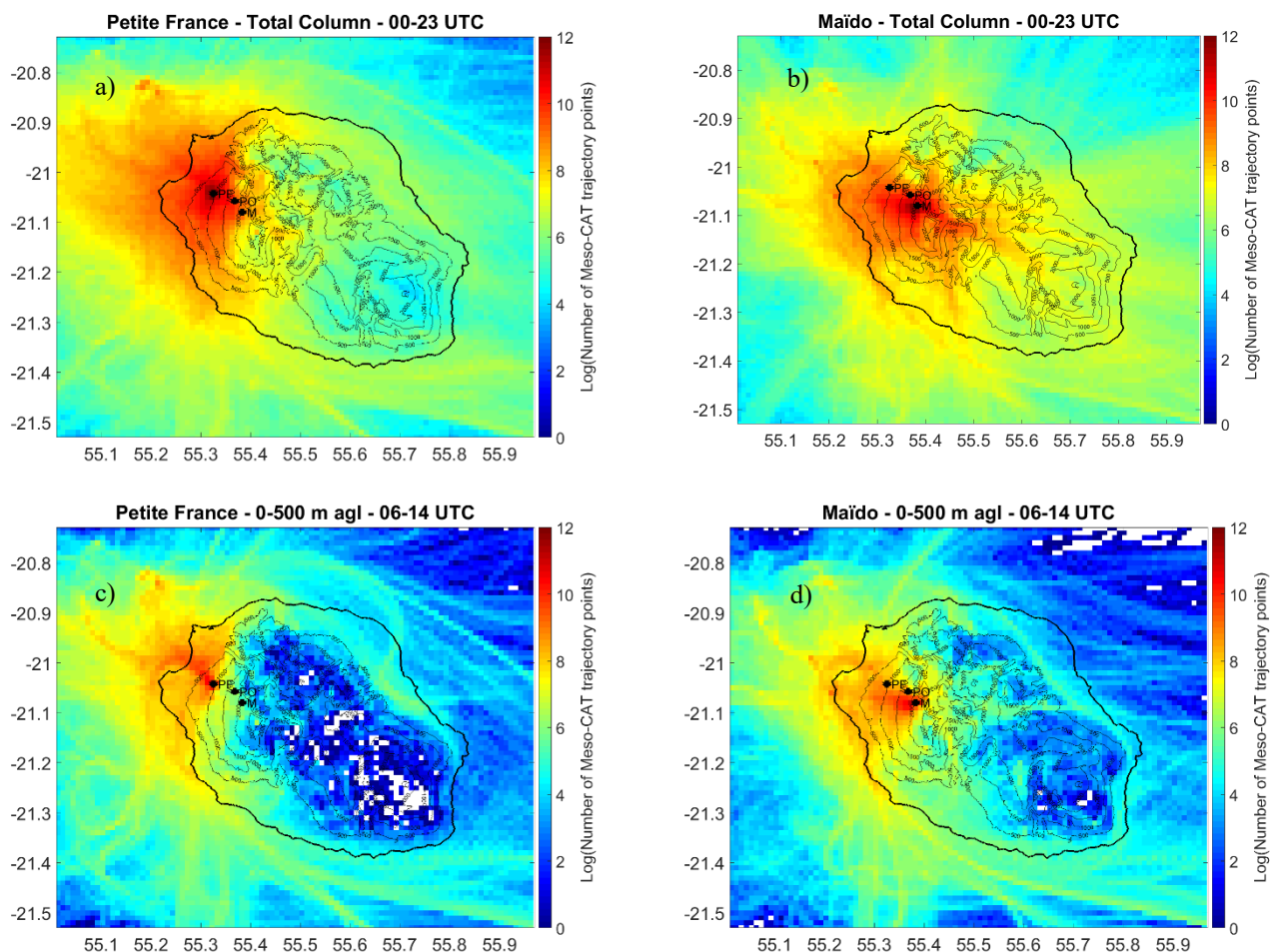


Figure 3. Natural logarithm of the number of back-trajectory points arriving at Petite France (left) and Maïdo (right) from 15 March to 8 April, per scare of 0.01° (around 1km) size. All trajectory points are taken into account for the calculation of the total column footprint maps (top), but only trajectory points between the ground and 500 m agl for the near surface footprint maps (bottom).

345 The connection between MO-5 and the other observation sites of the campaign is clearly evidenced by the footprints especially on 16 March and 1st April (Figure 4C of Rocco et al., 2022). As for PF-1, several trajectories also indicate an origin of the marine boundary layer. These specific periods will be studied preferentially to follow the lagrangian evolution of the chemical composition of the air mass.



3.2 Dynamical context for a typical cloudy day

350 An example of the dynamical context of the BIO-MAÏDO measurements is provided on 28 March 2019. Using back-trajectories and forward-trajectories computed with Meso-CAT, Rocco et al. (2022) and Dominutti et al. (2022a) were able to show that this situation was typical and highlighted the good connection between the observation sites.

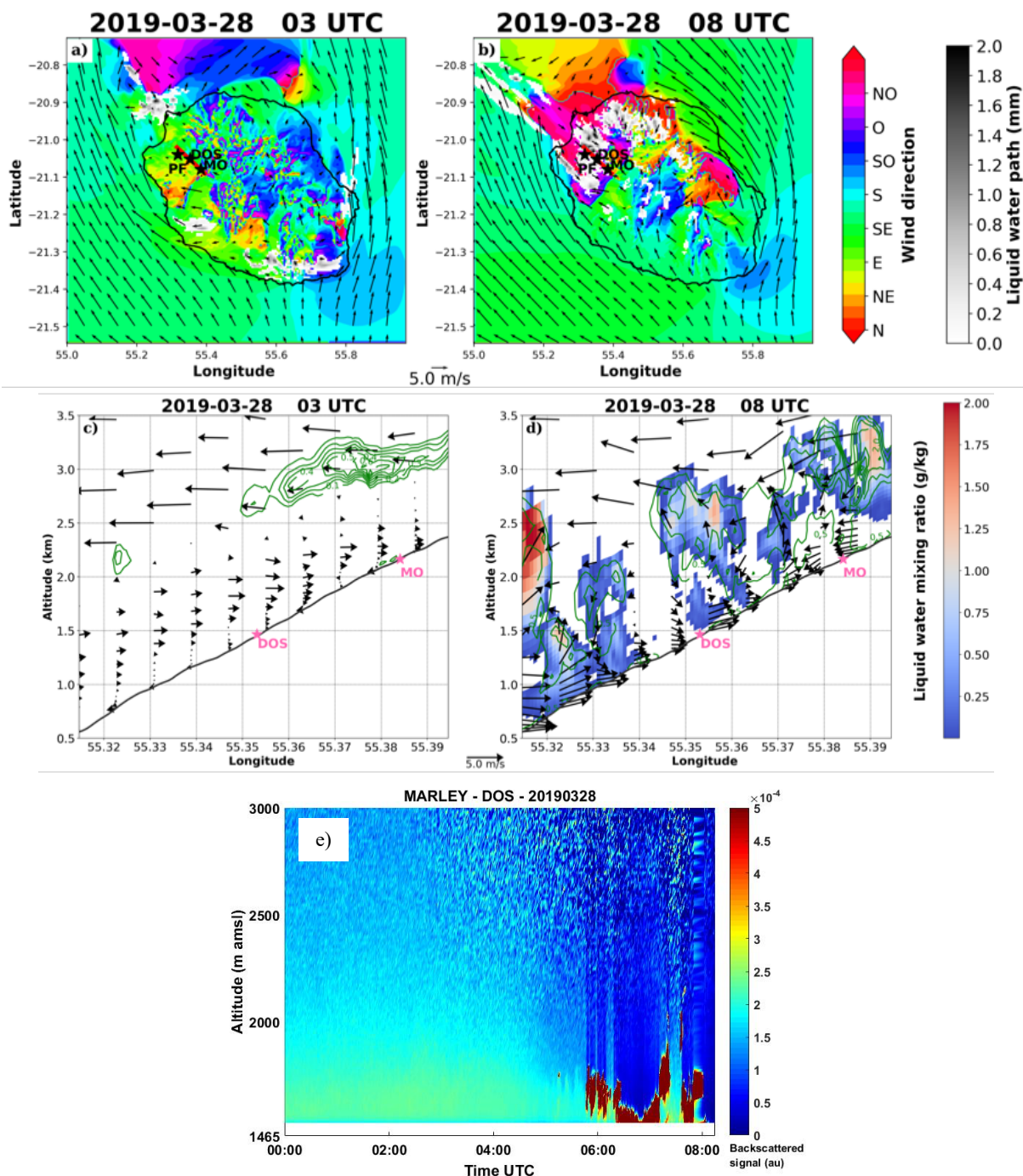


Figure 4. Meso-NH simulation: Horizontal cross-section at surface for wind direction (color scale) and intensity (vector in m s^{-1}) and liquid water path (mm, in grey) at 02 UTC (a), 08 UTC (b) for March 28. The vertical cross-section shows the liquid water mixing ratio (color scale in g/kg), wind direction and intensity (vector in m s^{-1}), and TKE (green isoline, in $\text{m}^2 \text{s}^{-2}$) at 02:00 UTC (c), 08:00 UTC (d) for March 28. (e) MARLEY backscattered signals at DOS-2.

355



Figure 4 shows the temporal evolution of the simulated low-level dynamics for the day of 28 March 2019 (500 m domain). The upper figures show the wind direction (color and vector) and intensity (vector size) at the surface at 03 UTC (a) and 08 UTC (b). During this day, the trade wind flow at the surface has a south-east component slightly disturbed by the presence of
360 cyclone Joania located at about 1000 km south-east of Reunion Island. Larger temporal (120 h) and spatial scale (the domain covers 40 to 75 °E) 5 days back-trajectories calculated with CAT and ERA5 ECMWF wind fields show that on 28 March, the air masses arriving to Réunion Island came from the active area of the cyclone whose center is located near 15°S,60°E on 24 March (see supplement material, Figure S1).

Classically, the trade wind flow bypasses the topography of Reunion Island with two zones of wind acceleration off the south-
365 west and north-east coasts of the island. At the very beginning of the morning (03 UTC), the trade winds return loop is located on the north of the island. This circulation does not penetrate inland (Fig. 4a).

At 08 UTC, the trade winds return loop moved northwest. There is a significant penetration of this surface flow as far as the DOS-2 station. MO-5 is located in a convergence zone between the overflow trade wind flow and this northwesterly counter-
flow (Fig 4b). In gray is represented the cloud water content integrated on the vertical. No cloud formation is modeled at 03
370 UTC apart from a few orographic clouds due to the uplift of the trade winds on the southern flank of the Piton de la Fournaise volcano. Over the BIO-MAÏDO area, the sky is clear (Fig. 4a). At 08 UTC associated to the ascent of the wind flow above the slopes of the Maïdo area, an important formation of clouds is stimulated. All the northwest of the island is concerned by the presence of clouds between 1000 m asl and 2000 m asl (Fig. 4b).

A vertical cross section (Fig. 4c and 4d) has been made in the axis of the red line of Fig. 4a and 4b. This cross section has used
375 the simulation results from the 100 m horizontal resolution domain at 03 UTC and 08 UTC. At 03 UTC (Fig. 4c), it is noticed that three wind layers have been modeled. Close to the surface, a catabatic wind flow is modeled along the slope. At about 500 m agl, a wind shear is modeled, and the airflow came from the north-west. This last layer is attributable to the return loop of the trade winds. Above, at about 2500 m agl, the wind direction is south-east due to the trade winds overflow above the island. At noon (08 UTC), the anabatic thermal breeze is clearly modeled. This wind regime is added with the trade wind return loop
380 on a 1 km thick layer (Fig. 4d). This up flow flux reaches 2000 m asl and we find again in the MO-5 area the convergence zone due to the trade winds overflow. As seen before, clouds are simulated over the slopes of the Maïdo area. This presence of clouds concerns almost the entire simulation domain (i.e. between 500 m asl and 2400 m asl). The base of the clouds has reached the surface between 700 m asl and 1900 m asl, therefore over an area covering all the measurement sites except MO-5. Figure 4e shows the time series of the MARLEY backscattered signal at the DOS-2 site for the 28 March until 08:15 UTC
385 (the system failed afterwards due to a power supply failure). The sky is clear until 06 UTC when the formation of clouds is triggered. The cloud base reaches the surface and the cloud top reaches 2200 m asl. These observations validate the simulated formation of clouds at DOS-2. Due to the dynamical transport above the slopes, these simulation results indicate that the air mass may have been loaded with chemical compounds in the aqueous phase before being evaporated near MO-5.



3.3 VOC measurements

390 During the BIO-MAÏDO campaign three PTR-MS were simultaneously installed for the first time in a tropical area to perform
 VOC mixing ratio measurements along the slope of the Maïdo road at PF-1, HM-3 and MO-5. In addition, during this
 campaign, characterization of VOC emissions from tropical and endemic/indigenous and exotic vegetation have been
 accomplished using solid sorbent cartridges for sampling followed by an analysis with Gas Chromatography – Mass
 Spectrometer and by Eddy covariance method and PTR-ToF-MS (Time-of-Flight PTR-MS) measurements on HM-3 site.
 395 VOCs measurements were firstly performed during the FARCE campaign in 2015 in Réunion Island (Dufлот et al., 2019);
 concentrations of isoprene were measured at different locations of the island. In this study, the maximal concentrations of
 isoprene were measured in the 100 to 200 pptv range in the tropical forest site (Bélouve forest). From 2018 to 2021, a PTR-
 MS was installed at MO-5 for continuous VOCs measurements as part of the OCTAVE project. These measures have been
 used in the Verreyken et al., (2020) that addressed the impact of long-range biomass burning at remote sites at MO-5 and an
 400 overview of the 2-year campaign is presented in Verreyken et al., (2021). In this last study, high levels of BVOC have been
 observed and isoprene concentrations reached up to 500 pptv. In addition, during the OCTAVE project, a second PTR-MS
 was positioned in the Bélouve forest (20.9° S, 55.3° E, 7 m asl.) and at Le Port (21.06° S, 55.5° E, 1498 m asl) sites for 10
 days each in April-May 2018. In a study dedicated to the analysis of formaldehyde sources and origin at MO-5 using these
 additional measurements, Rocco et al. (2020) found that most of formaldehyde is formed from biogenic secondary compounds
 405 (oxidation of biogenic VOCs with 37% in average).

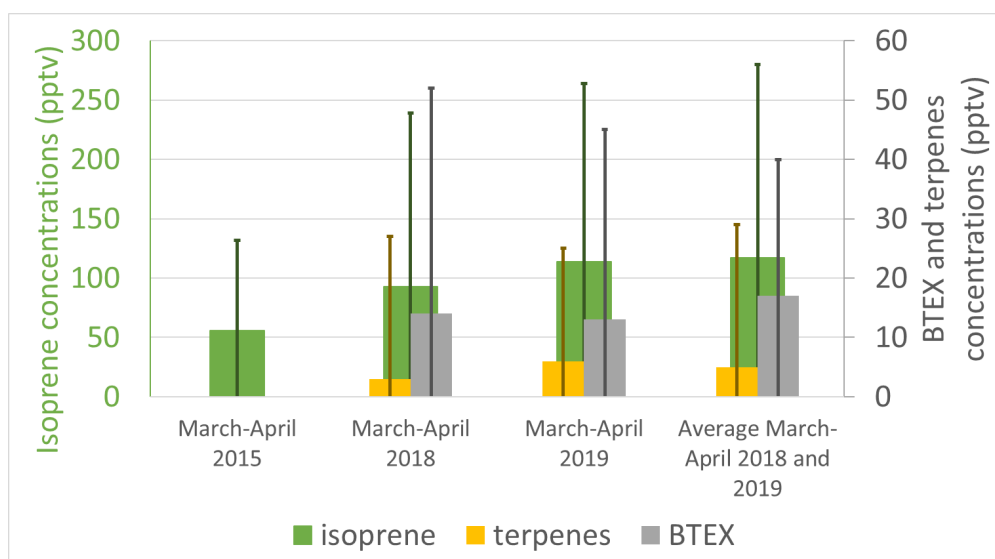


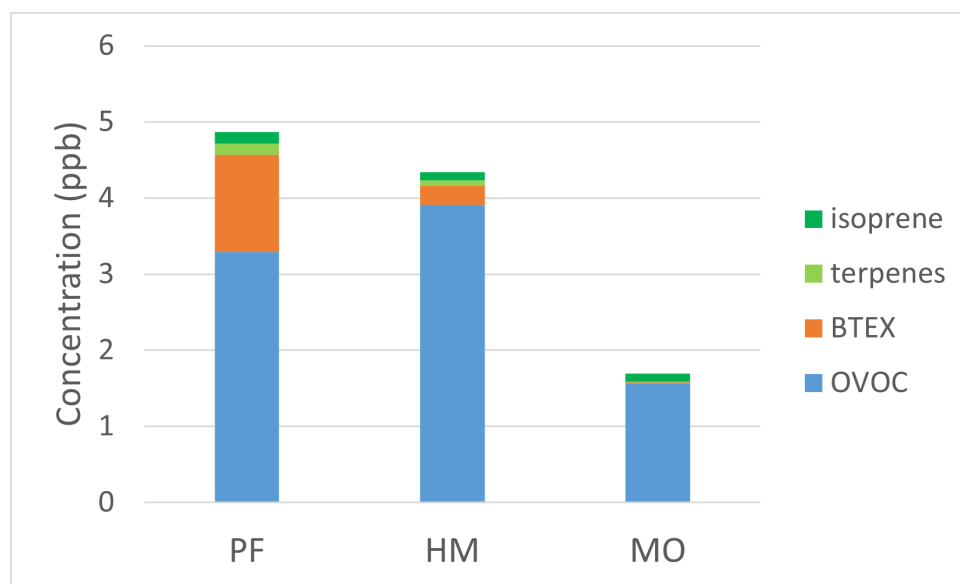
Figure 5: Isoprene, terpenes and BTEX mixing ratio (pptv) for the FARCE (2015, Dufлот et al., 2019), OCTAVE-1 (2018, Rocco et al., 2020), BIO-MAÏDO (2019, Rocco et al., 2022) and OCTAVE-2 (March-April 2018-2019, Amelynck et al., 2021) at the Maïdo Observatory.

410 Figure 5 compares averaged mixing ratios of isoprene, terpenes and BTEX (sum of benzene, toluene, ethylbenzene and xylenes) at MO-5 for four datasets corresponding to FARCE, OCTAVE-1 (first – 2018 datasets) BIO-MAÏDO, and OCTAVE-



2 (2018 and 2019 datasets) campaigns. Dominant mixing ratios are observed for isoprene all over the different campaigns with averaged concentrations of 95 ± 133 pptv. Low mixing ratio of terpenes and BTEX are measured at MO-5 showing low influence of anthropogenic emissions and low emissions of monoterpenes by local vegetation. Level of isoprene are higher for BIO-MAÏDO and the second set of OCTAVE than for FARCE and the first set of OCTAVE. For FARCE campaign, terpenes and BTEX are not available. Terpenes are the highest for BIO-MAÏDO and BTEX are the smallest but with comparable levels with other datasets.

The coupling of VOCs chemistry and dynamics measured during BIO-MAÏDO campaign was investigated to better understand the role of dynamics in the distribution of VOCs (Rocco et al., 2022). This new and first approach combined cover land footprint and backward trajectories. It provided information on the nature of the ground-surface influencing the air masses during the few days and hours before the air mass arrives at the sampling sites (PF-1 and MO-5). The variability of VOC concentrations along the slope was also analyzed. The origin of air masses greatly varied among days. They showed differences in forward and backward trajectories coming from PF-1 to MO-5 with air masses more or less advected from the down-slope areas. Many days were marked by a frequent oceanic air mass origin (up to 50%) with high concentrations of methanol and acetone. Ratio of isoprene oxidation products to isoprene concentration have been calculated. Calculated ratios were in average 0.44 ± 0.42 at MO-5 and 1.11 ± 1.59 in PF-1. A lower ratio at MO-5 indicates recent emissions of isoprene, and therefore a major contribution from the local vegetation, which has not yet had time to oxidize to secondary compounds.



430 **Figure 6. Average concentration of isoprene, terpenes, OVOC and BTEX concentration in ppb at Petite France (PF-1), Hotel du Maïdo (HM-3) and at the Maïdo observatory (MO-5).**

Figure 6 shows the average composition of isoprene, terpenes, OVOC (sum of methanol, acetaldehyde, acetone and methyl ethyl ketone/MEK) and BTEX mixing ratios at PF-1, HM-3 and MO-5 averaged during the whole BIO-MAÏDO campaign. A spatial gradient in total VOC mixing ratios is observed from PF-1 to MO-5 with a decrease by a factor of 2.5 between PF-1



and MO-5. OVOCs are the major contributors to total VOC burden (> 50% in vol); while the contribution is getting lower for
435 primary biogenic and anthropogenic VOC from PF-1 to MO-5 where OVOC is dominant. This gradient depends on the
distance to the main primary sources (i.e. vegetation and traffic), air mass history during its transport (cloud presence, surface
characteristics) and air mass aging.

During BIO-MAÍDO campaign, mixing ratios of isoprene measured at the 3 sites are between 100 and 600 pptv. Average
isoprene mixing ratios for the period was 0.16 ± 0.12 ppbv, 0.11 ± 0.10 ppbv and 0.12 ± 0.15 ppbv at PF-1, HM-3 and MO-5
440 respectively. Terpene's mixing ratios are 20 times higher in PF-1 than MO-5, reaching a value of 140 pptv. As PF-1 is a mixed
rural and urban site, the sources of terpenes are more abundant in this site than in MO-5. At HM-3, averaged concentrations
of α -pinene, β -pinene and limonene were respectively 0.06 ± 0.04 ppbv, 0.01 ± 0.01 ppbv and 0.09 ± 0.05 ppbv. As marker
of anthropogenic emissions, BTEX are also present in higher level at PF-1 (1.27 ± 0.67 ppbv) than at MO-5 and HM-3. Dilution
and oxidation processes explain the decreasing levels due to the increased distance to the source. Other hypotheses must be
445 considered. Despite BTEX are poorly soluble in water, BTEX was detected in every cloud water samples with a mean
concentration of 4.2 nM (Dominutti et al., 2022) showing that clouds act as a sink for aromatic compounds. Another potential
sink is the deposition of BTEX on the leaf cuticle through gaseous deposition (Molina et al, 2021). Finally, Rocco et al., (2022),
showed that PF-1 and MO-5 was not dynamically connected every day during the campaign. Concerning the OVOC, the
species in higher mixing ratios for the three sites is methanol with an average mixing ratio of 2.16 ± 0.89 ppbv, 2.79 ± 1.10
450 ppbv and 0.82 ± 0.35 ppbv at PF-1, HM-3 and MO-5 respectively. As this compound is primarily emitted from terrestrial plant
during the growth and the decay stages (Bates et al., 2021 and references therein), this can explain the highest mixing ratio
observed at HM-3.

3.4 Aerosol measurements

An online ToF-ACSM was used to determine the chemical composition of non-refractory- PM_{10} (NR- PM_{10}) aerosol at MO-5,
455 providing mass concentrations for organic, sulphate, nitrate, ammonium and chloride species. At MO-5 this instrument
operated continuously from March 13th to April 2nd and showed an average NR- PM_{10} mass concentration of $4.6 \pm 6.2 \mu g m^{-3}$
with a strong diurnal variability. Daily mass concentrations reaching up to $25 \mu g m^{-3}$ were observed at the start and the end of
the field campaign, while nighttime concentrations, when the site was most likely in the free troposphere, were close to the
limit of detection of the instrument. These measurements were coherent with aerosol number concentrations measured by
460 DMPS that showed similar diurnal profiles with typical signatures of new particle formation on a daily basis (Rose et al.,
2019).

The NR- PM_{10} were dominated by SO_4^{2-} (57.3%), followed by organics (23.3%), NH_4^+ (14.2%), and NO_3^- (2.2%) (Dominutti et
al., 2022b). The high concentration of sulfate containing particles and the low concentration of NH_4^+ , show that forms of
sulfate, other than ammonium sulphate ($(NH_4)_2SO_4$), were sampled, likely acidic aerosol such as NH_4HSO_4 or eventually in
465 the form of organosulphates (Brito et al., 2018).



The contribution of different organic species to the total organic mass concentration was determined using positive mass factorization (PMF), with the source finder (SoFi) tool (Canonaco et al., 2013). Three factors were resolved using PMF analysis on the entire organic matrix from m/z 1 to 150; a more oxidized organic aerosol (MOOA) (75%), a primary organic aerosol (POA) (18.5%), and an isoprene derived organic aerosol (IEPOX-OA) (11%).

470 During the second part of the field campaign, air masses were exposed to aqueous phase processing (as determined using the results of Meso-NH model). Using this information, aerosol chemical composition and physical properties were compared under both clear and cloudy conditions. A clear shift in the aerosol size distribution was observed (an increase by 15% of Aitken and accumulation mode aerosols under cloudy conditions), as well as a shift in the organic aerosol chemistry with increases in MOOA, in oxalic acid concentrations and in sulfate aerosols in the PM_{10} offline filters. These observations together
475 with model estimates of in-cloud processing of aerosols suggest that oxidation of gaseous precursors, and primary organic aerosol species and other aqueous phase processing have a significant impact on the sources of organic aerosol (notably oxalic acid), and on aerosol physical properties (Dominutti et al., 2022b).

Additionally, PM_{10} aerosols were simultaneously sampled by offline filters at MO-5 and PF-1 during the whole field campaign. Figure 7 present the average concentrations of different PM_{10} components observed at MO-5 and PF-1 during the BIO-MAÏDO
480 field campaign, split between daytime and nighttime.

The average PM_{10} concentrations showed significant differences between the MO-5 and PF-1 sites. The main discrepancies were observed for total organic matter (OM) concentrations, which were higher at PF-1 (3480 ng m^{-3}) than at MO-5 (1506 ng m^{-3}) by a factor of 2.3 (Fig. 7a and 7b). In addition, higher concentrations at PF-1 were also observed for Na^+ and NO_3^- (by a factor of 2) and Cl^- and EC (by a factor of 3.6 and 4.5, respectively) (Fig. 7a and 7b). These differences could be related to the
485 distance of the sites from emission sources, as is the case of marine origin ions Cl^- and Na^+ , and the traffic-related ones, EC and NO_3^- . On the other hand, sulfate and ammonium being associated with long range transport, do not differ significantly in the average concentrations of the sites. A second large difference comes from the fact that MO-5 is in free tropospheric conditions during the night, leading to much larger differences in the day/night ratios at MO-5 than at PF-1. Notably, OM at PF-1 does not show a substantial difference between daytime and night-time (2.01 and $1.81 \text{ } \mu\text{g m}^{-3}$, respectively), however, its
490 concentrations were dissimilar at MO-5 (0.90 and $0.35 \text{ } \mu\text{g m}^{-3}$, respectively).

The OM composition was also variable between the sites and also on a day/night basis (Fig. 7c). As expected, sugars alcohols and monosaccharides had higher concentrations at PF-1 than MO-5, by a factor of 3 to 10. Mean concentrations at PF-1 were determined by arabitol (49 ng m^{-3}), levoglucosan (38.6 ng m^{-3}), mannitol (35.5 ng m^{-3}), and glycerol (19.3 ng m^{-3}). At MO-5, a similar profile is observed but differently controlled by levoglucosan (8.8 ng m^{-3}), mannitol (6.5 ng m^{-3}), trehalose (4.9 ng m^{-3}), and arabitol (4.4 ng m^{-3}). Interestingly, higher concentrations of sugars were observed at night at PF-1 (Fig. 7c),
495 suggesting that environmental conditions (such as temperature and humidity) can have a role in the emission processes of these compounds by natural sources (e.g., soils, bioaerosols, plants and fungal spores). Zhang et al., (2010) found that arabitol and mannitol in PM_{10} showed significant correlations with relative humidity and air temperature, suggesting a wet emission mechanism of biogenic aerosol in the form of fungal spores in a tropical rainforest. The sugar alcohols, mannitol and arabitol,



500 are common energy reserves in fungi and are produced in large amounts by many fungi (Golly et al., 2019, Zhang et al 2010, Bauer et al 2008). In contrast, levoglucosan, a degradation product from biopolymers, is known as a good molecular tracer of biomass burning in the literature (Simoneit et al., 2002). However, levoglucosan concentrations observed in our study are more likely to be due to domestic biomass burning (e.g. cooking emissions) rather than forest fires (not reported in the area during the campaign). Thus, our results show a strong contribution of biogenic sources on PM₁₀ samples such as fungi spores, soils, and microorganisms and to a lesser extent the contribution from biomass burning aerosols.

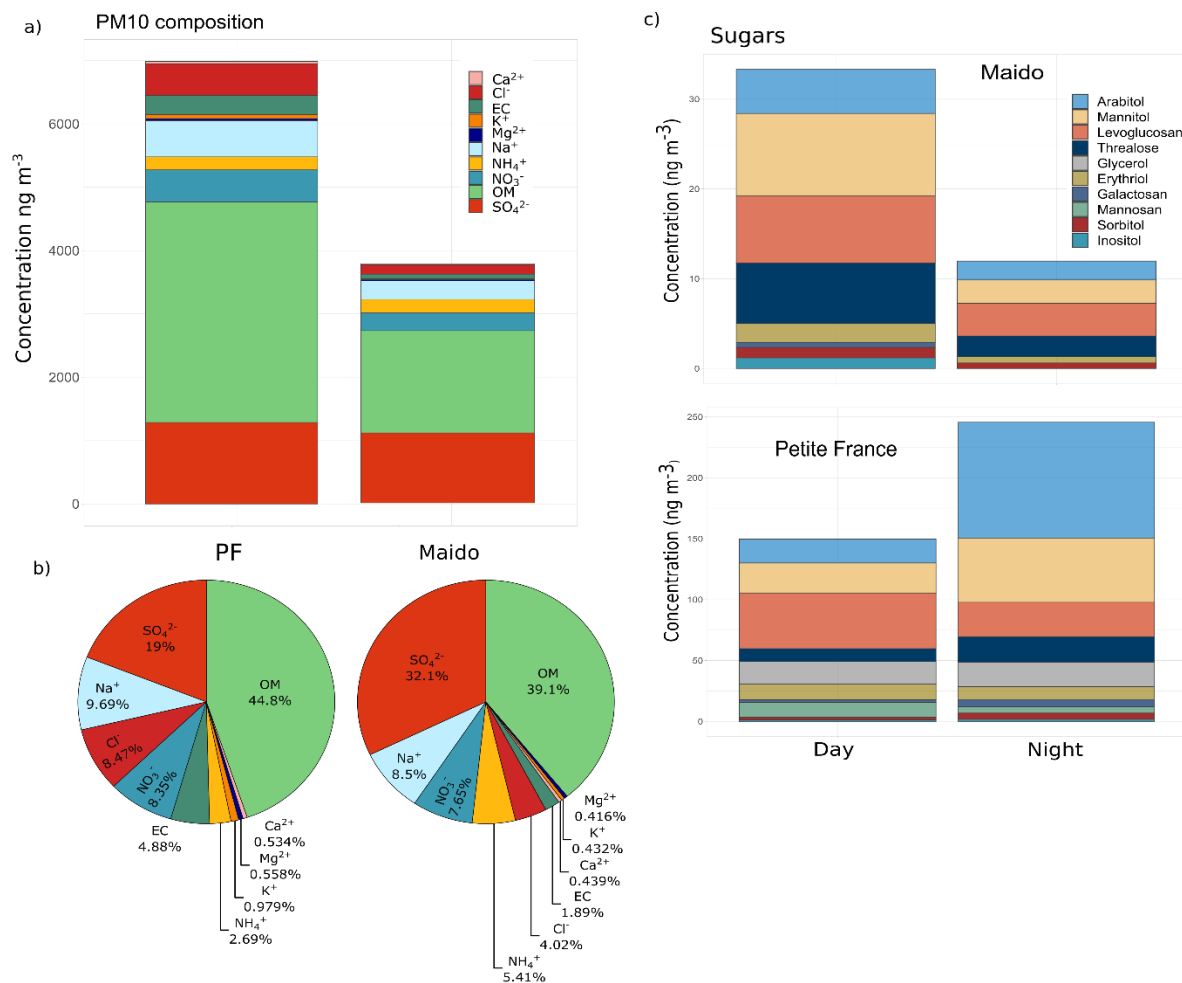


Figure 7. (a) Average PM10 composition observed at Petite France (PF-1) and Maido Observatory (MO-5), (b) Relative contribution of PM10 components during daytime observations and (c) average sugars concentrations at PF-1 and MO-5 sites during day and nighttime.

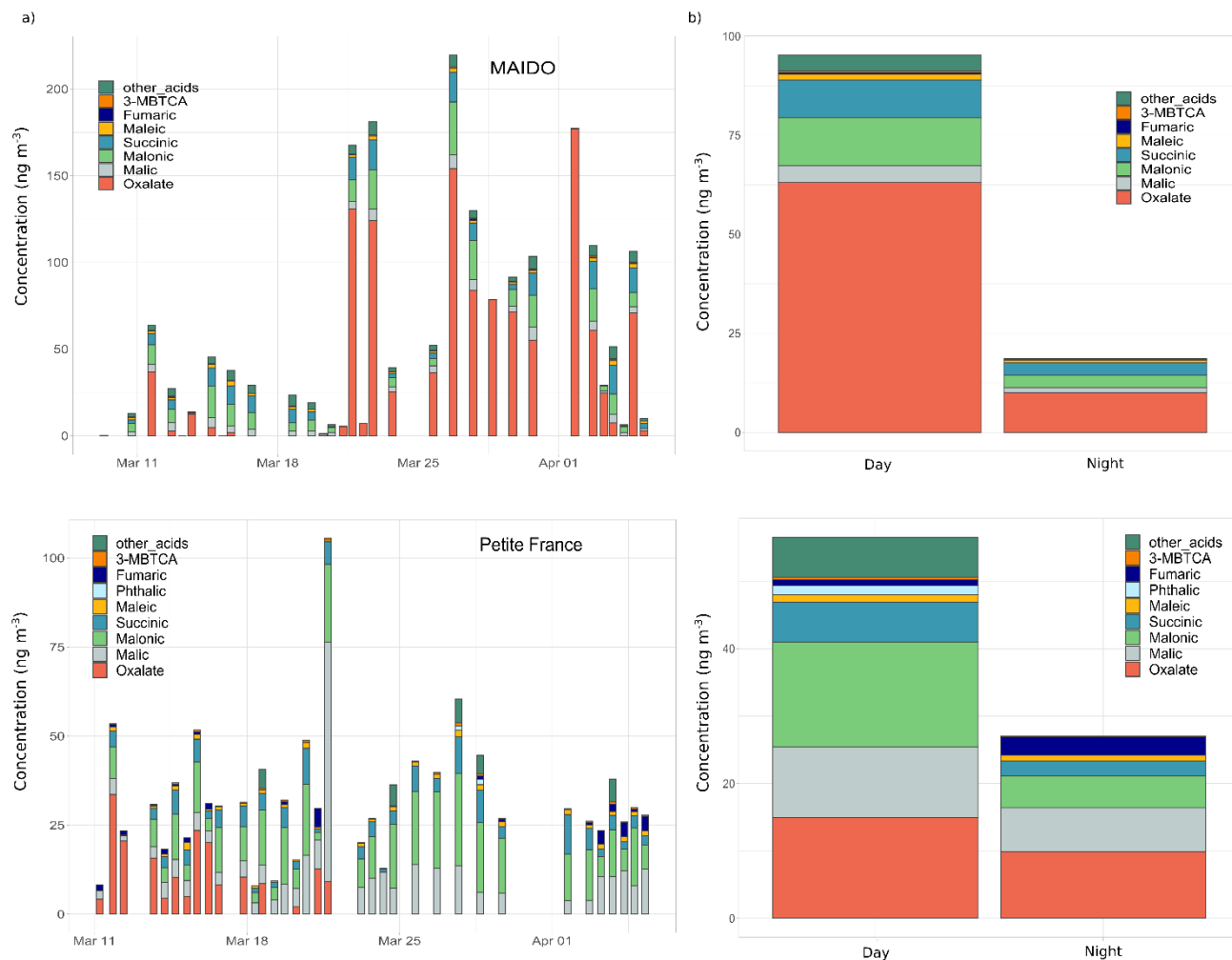


Figure 8. (a) Time series evolution of organic acid concentrations observed at MO-5 and PF-1 and (b) average concentrations observed at each site during day and night observations.

Seventeen organic acids concentration were measured at both sites (Fig. 8). Contrarily to what was observed for ions and sugars, higher mean concentrations of total organic acids were obtained at MO-5 (95.3 ng m^{-3}) than PF-1 (56.5 ng m^{-3}). The largest contribution at both sites was from oxalate, which presented average daytime concentrations of 63 ng m^{-3} at MO-5 and 15 ng m^{-3} at PF-1. Oxalic acid is the most abundant and ubiquitous dicarboxylic acid (Kawamura and Bikina, 2016) and is commonly associated as secondary organic tracer formed from the photochemical/aqueous oxidation of many organic precursors (Ervens et al., 2011). As discussed by Dominutti et al., (2022b), the large contribution of this acid at MO-5 suggests the impact of more oxidized aerosols transported over long distances. Organic acids also include the presence of other dicarboxylic acids, such as malonic, malic and succinic, species typically observed in other and similar environments (Kawamura and Bikina, 2016, Golly et al., 2019, Cheng et al., 2013, Wang et al 2006). The average daytime concentrations of malonic were similar at both sites (15.6 and 12.1 ng m^{-3} at PF-1 and MO-5, respectively), however, succinic (5.9 and 9.6



ng m⁻³ at PF-1 and MO-5, respectively) and malic (10.4 and 4.2 ng m⁻³ at PF-1 and MO-5, respectively) exhibited some small
525 differences between sites. These acids can be emitted into the atmosphere from various anthropogenic (e.g. vehicular, biomass
burning) and natural (marine aerosols) sources, but there are mainly produced in the atmosphere by several photochemical
reactions of their organic precursors. The involvement of the photochemical process in the production of those acids can be
evaluated by the mass ratio of malonic to succinic acid (<1 for photochemically aged aerosols, Kawamura and Sakaguchi,
1999). Our observations show average malonic/succinic ratios of 2.62 and 1.51 at PF-1 and MO-5, respectively, confirming
530 the presence of photochemical aged aerosols in Réunion Island.

Overall, the chemical profiles and PM₁₀ concentrations show that the MO-5 and PF-1 sites are rather disconnected during most
of the field campaign, especially at night. The results reveal that different environmental conditions and atmospheric dynamics
have an impact on the spatial distribution and composition of aerosols in Reunion Island.

3.5 Cloud chemistry analysis

535 During the BIO-MAÏDO campaign, 14 cloud samples were collected at PO-4 and characterized by physico-chemical and
microbiological analysis. This section is devoted to summarize the main results described in detail in Dominutti et al. (2022a)
and to present the ongoing works.

Data obtained with the cloud droplet probe (CDP) reveal that clouds collected on the slope of the mountainous island present
low water content with LWC values of 0.07 ± 0.04 g m⁻³ on average. Those values are more representative of LWC reported
540 for fogs than the higher ones reported for marine clouds (values closer to 0.2 to 0.4 g m⁻³), such as those sampled at Puerto
Rico (Gioda et al., 2013) or Cape Verde (Triesch et al., 2021). This is to the atmospheric dynamical circulation that leads to
the formation of clouds with low LWC over this part of the island (see section 3.2 and Dufлот et al., 2019). Concerning the
size of the droplets, the D_{eff} for the 14 cloud events is rather small, with an average value of 13.7 ± 1.51 μm (Figure 9a).

The main inorganic ions have been quantified in priority since they are used as tracers of various natural and anthropogenic
545 sources (Deguillaume et al., 2014). In line with the low LWC, the total concentrations of these ions are little diluted and
therefore high, with concentrations ranging from 600 to 4370 μmol L⁻¹. As expected, for all the cloud events, a major influence
of ions from marine origin is found, confirming the contribution of sea salt to the cloud formation (Na⁺: 490 ± 399 μmol L⁻¹;
Cl⁻: 434 ± 370 μmol L⁻¹) (Figure 9b). Those amounts are similar to those observed for other marine sites. Nitrates are the third
ions in relative contribution, with a concentration of 239 ± 168 μmol L⁻¹. These elevated concentrations may be linked to local
550 anthropogenic sources (uptake of NO_x/nitric acid from the gas phase into the droplets or dissolution of nitrate from aerosols).
This additional anthropogenic fraction is confirmed by the presence of sulfate in a significant quantity (118 ± 44 μmol L⁻¹).
The measured SO₄²⁻/Na⁺ ratio is much higher than the standard sea-salt molar ratio by a factor of 2.8 on average, confirming
anthropogenic contribution to the sulfate amount. The contribution to the sulfate concentration of volcanic emissions through
the dissolution of SO₂ in cloud droplets and oxidation to form sulfates cannot be ignored, even if no eruption was reported
555 during the sampling period. Ammonium levels (123 ± 43 μmol L⁻¹) are comparable to the observations conducted for remote
continental sites, indicating plausible terrestrial/agricultural inputs. The concentration of these compounds determines cloud



water acidity, leading to acidification (i.e., SO_4^{2-} , NO_3^-) and/or basification (i.e., NH_4^+ , Mg^{2+} , K^+ , Ca^{2+}) together with the CO_2 dissolution from the gas phase. The pH of the cloud samples does not vary a lot, with values ranging from 4.7 to 5.5. Finally, trace metals have been quantified and present very low concentrations. Mg and Zn, which have natural origin such as sea salt, present the most important concentrations, followed by Cu, Fe, Mn, Ni, Sr, and V. These amounts are in the same range as previous studies performed in marine environments (Fomba et al., 2013, 2020) or influenced by marine emissions (Bianco et al., 2017). Iron speciation has been evaluated with Fe(II)/Fe(II)+Fe(III) ratio equal to $52 \pm 22\%$. This suggests an efficient conversion of Fe(III) to Fe(II) and possible complexation of Fe(III) with organics, leading to its stabilization under this redox form. Nonetheless, the effect of iron on the oxidative budget is expected to be low due to low Fe concentrations (0.88 ± 0.19 $\mu\text{mol L}^{-1}$ on average).

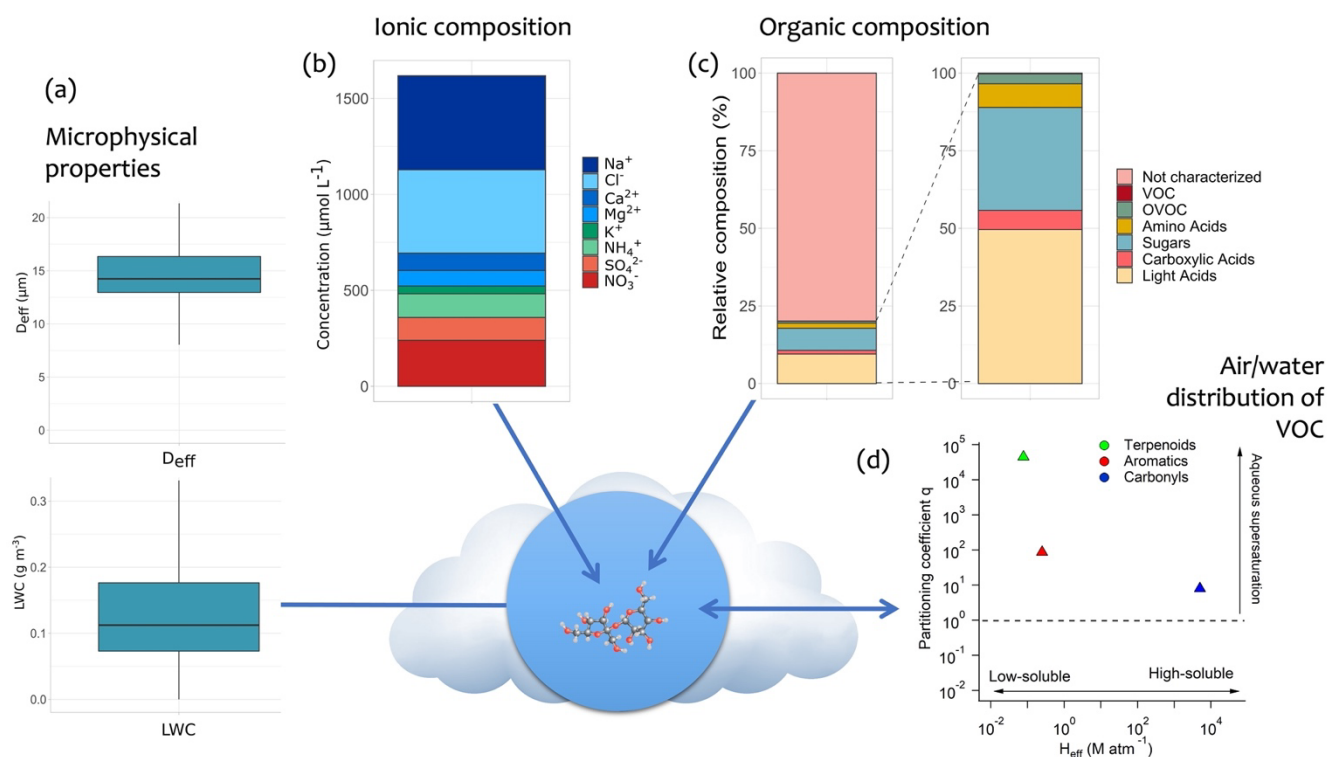


Figure 9. Summary of the main results of the cloud water chemical characterization: (a) Microphysical properties (LWC and D_{eff}), (b) concentration of the main inorganic ions, (c) relative organic composition, (d) partitioning coefficient q of VOC between the gaseous and aqueous phase as a function of effective Henry's law constant (H_{eff}).

Dissolved organic compounds have also been intensively investigated during the campaign. The average concentration of dissolved organic carbon (DOC) is equal to 25.5 ± 19.2 mg C L^{-1} that is much higher than values reported for cloud waters sampled in marine environments such as at the southern Pacific Ocean (Benedict et al., 2012), Puerto Rico (Reyes-Rodriguez et al., 2009), southern Asia (Stahl et al., 2021) or the puy de Dôme station for clouds under the marine influence (Deguillaume et al., 2014). Like for inorganics, this indicates additional inputs of DOC other than sea-related ones. Among the quantified



575 compounds, organic acids and sugars contribute on average to a significant fraction of the DOC (around 18%) (Figure 9c).
Light carboxylic acids, such as formic and acetic acids, are dominant compounds and present concentrations higher than those
observed in marine environments. Results indicate that their concentration in the aqueous phase is mainly due to mass transfer
from the gas phase, in which they are emitted by anthropogenic and biogenic primary sources. The most concentrated
dicarboxylic acids are lactic and oxalic acids, resulting from the reactivity in the aqueous phase or from the dissolution of the
580 CCN. Reported concentrations of dicarboxylic acids are rather low compared to other sites, probably because clouds freshly
form over the mountain slope, which does not allow their efficient production by aqueous reactivity. Sugars are also ubiquitous
in all our samples and derive mainly from the water-soluble fraction of the CCN. The aqueous concentration of sugars is equal
on average to $22.2 \pm 15.4 \mu\text{mol L}^{-1}$ and the calculated atmospheric concentration ($121.3 \pm 69.6 \text{ ng m}^{-3}$) is important compared
to previous aerosol studies (Verma et al., 2018; Zhu et al., 2015). This can be explained by the importance of biogenic
585 emissions at Réunion Island but potentially also by the production by microorganisms in cloud water. Identically to sugars,
amino acids are issued from biogenic production. They have been measured with total concentrations of free amino acids
(TCAA) varying from 0.8 to $21.1 \mu\text{mol L}^{-1}$ (average: $4.6 \pm 5.5 \mu\text{mol L}^{-1}$), representing 1.6% of the DOC in average. These
values are higher than those reported at a marine site in Cape Verde by Triesch et al. (2021) and much higher than those
measured at the puy de Dôme station (Renard et al., 2022). This fact can be explained by the surrounding potentially important
590 sources (sea surface but also vegetation). Among the 15 amino acids detected, Serine, Alanine, and Glycine are dominant; a
plausible explanation is related to their high atmospheric lifetimes due to low reactivity with hydroxyl radicals and their
preponderance in biological matrices. Finally, carbonyls (OVOC) and low solubility VOC have been investigated. The average
concentration of carbonyls is $3.5 \pm 1.7 \mu\text{mol L}^{-1}$ (on average: 42.0% of formaldehyde, 14.2% of hydroxyacetaldehyde, 11.3%
of acetaldehyde, 10.4% of acetone, 9.8% of glyoxal, 6.9% of hydroxyacetone and 5.3% of methyl glyoxal), representing 1%
595 of the DOC on average. This global amount is rather low compared to other studies, and the formaldehyde to acetaldehyde
ratio suggests a contribution of vegetation emissions. Terpenoids (α -pinene, β -pinene, and limonene) and isoprene have been
detected together with primary aromatics (benzene, toluene, ethylbenzene, xylenes) in nmol L^{-1} range, contributing to 0.35%
of the DOC. Despite their low concentrations, they are of interest since they are tracers of emissions and allow for evaluation
air/droplet partitioning (see below).

600 The contribution of the organic compounds targeted in this project represents around 20% on average of the DOC
concentration, reaching up to 35% for one specific cloud. This reveals the complexity of the cloud organic matter that has been
recently highlighted by high-resolution mass spectrometry (Cook et al., 2017; Bianco et al., 2018; Sun et al., 2021). Thousands
of molecular formulae have been detected in cloud water, and their presence and concentration are related to the influence of
primary sources and atmospheric processing. The analysis by FT-ICR MS requires at least 50 mL of cloud water, which is
605 thereafter pre-concentrated and desalted by solid-phase extraction. Three samples (R8, R9, and R10B) presented enough
volume to be analyzed with this technique. Two complementary ionization sources focused the attention on different organic
compounds: electrospray ionization in positive and negative polarities enabled the identification of polar and semipolar
compounds, while atmospheric pressure photoionization (APPI) revealed the presence of less polar compounds, probably



related to lipids and terpenes. The assigned molecular formula retrieved by high-resolution mass spectra does not enable the attribution of a structural formula. Nevertheless, based on the elemental composition, considering the number of carbon, oxygen, nitrogen, hydrogen, and sulfur atoms, the molecular formula can be classified into compounds of biogenic and anthropogenic origin, such as lipids, carbohydrates, proteins or unsaturated hydrocarbons and condensed aromatics, respectively. This analysis offers the possibility of getting information on the DOC fraction not characterized by previously presented targeted analysis. The detailed presentation of FT-ICR MS results will be reported (work in progress). In addition to the chemical characterization, specific attention has been paid to the distribution of VOC between the gas and the aqueous phase in the cloudy atmosphere and to the environmental variability of the chemical composition. For OVOC, a small deviation from Henry's law equilibrium has been observed. However, high supersaturation in the aqueous phase is measured for low soluble biogenic and anthropogenic compounds as previously described in van Pinxteren et al. (2005) and Wang et al. (2020) (Figure 9d). Possible explanations are interactions of these compounds with dissolved or colloidal matter or adsorption at the air-water interface.

A statistical analysis has been performed combining cloud chemical data with back-trajectory calculations derived from Meso-CAT associated with the Corine 2018 land-cover database. This work shows that air mass origin and microphysical variables cannot explain the evolutions observed in cloud chemical composition. This reveals the complexity of interconnected processes occurring on the mountain slopes (i.e. emission sources, multiphasic transfer, and chemical processing in clouds).

3.6 Biological measurements: cloud water and aerosols

The diversity of culturable bacteria from clouds collected at PO-4 during this campaign are reported, along with others, in Charpentier et al. (submitted, 2022). These included 105 distinct strains, most of which (58%) were affiliated with Proteobacteria (39% Gammaproteobacteria, 12% Alphaproteobacteria and 7% Betaproteobacteria), followed by Actinobacteria (34%) and Firmicutes (7%). The most represented species comprised *Stenotrophomonas*, *Pseudomonas* and *Acinetobacter* in Gammaproteobacteria, *Microbacterium* and *Curtobacterium* in Actinobacteria, *Bosea* and *Sphingomonas* in Alphaproteobacteria, and *Bacillus* in Firmicutes. This is a common pattern for viable bacteria in atmospheric samples (e.g., Vařtilingom et al., 2012).

Bacteria diversity profiling by high-throughput sequencing from 74 aerosol samples collected at PF-1 and Mařdo indicated the presence of 8,437 OTU_{0.03} (operational taxonomy units clustered at 97% sequence similarity, i.e. ~ prokaryotic species level see Amato et al. (2017) for details) in total, of which 6,935 were affiliated at >95% identity to know sequences in databases. The vast majority of these (99.6%) were bacteria, the remaining being attributed to Archaea. As for culturable bacteria from clouds, the phylum Proteobacteria dominated (29.3% of the sequences), before Firmicutes, Actinobacteria and Bacteroidetes represented each by ~16% of the sequences. Among others, Cyanobacteria, Planctomycetes and Acidobacteria notably contributed each 3% to 4% of the sequences. This composition is consistent with airborne bacteria at other places of the planet using similar methods (e.g. Amato et al., 2017; Péguilhan et al., 2021).



4. Discussion

Online measurements of VOC during the campaign show, as expected, the presence of BVOC dominated by isoprene along the slope of the Maïdo and at the observatory during the daytime. The effect of cloud on mixing ratios of isoprene and its oxidation products is clear looking at their diurnal variation for cloudy days (See Fig. 4 in Rocco et al., 2022). It is well-known
645 that clouds induce less efficient emission of isoprene due to the decrease of solar radiation and temperature (e.g. Guenther et al., 1993), but the scavenging of isoprene and its oxidation products in cloud droplets could also contribute to their decrease. Dominutti et al. (2022a) have shown that isoprene has been detected in almost all the samplings of cloud water during the campaign (at concentration of about a few dozen nmol L⁻¹). Furthermore, despite BTEX are poorly soluble in water, BTEX were detected in every cloud water samples with a mean concentration of 4.2 nmol L⁻¹ showing that clouds act as a sink for
650 aromatics compounds. However, even if the level of oxidation products from isoprene decreases from PF-1 to MO-5 for days where both sites are dynamically connected, VOC measurements do not allow determining the importance of the photochemistry versus the dilution and the deposition on the air mass composition sampled at MO-5 (Rocco et al., 2022).

The analysis of PM₁₀ filters shows that, even if the concentration of organic matter (OM) is lower at MO-5 than at PF-1, the concentration of dicarboxylic acids is the highest at MO-5 especially in the second part of the campaign where oxalate is
655 detected only at MO-5 (Fig. 8a), and which was cloudier. The PMF analysis of the submicron aerosols at MO-5 show that the more oxidized organic fraction of aerosols (MOOAs) is the dominant part of the organic aerosol, and its contribution increases during the second part of the campaign (Dominutti et al., 2022b). These results seem to underline the possible effect of cloud processing on the organic composition of particles sampled at MO-5. An analysis combining observations of PM₁₀ composition, aerosol size distribution, contribution of PMF factors and results of simulated clouds along the slope from Meso-
660 NH model highlights the role of cloud processing on aerosols sampled at MO-5 (Dominutti et al., 2022b). Observations showed a shift to larger diameter of the aerosol size distribution (15% for Aitken and accumulation modes) and an increase of 10% of the contribution of sulfate and MOOAs in the chemical composition of submicron particles when cloud processing occurs during the daytime (Dominutti et al., 2022b).

The database from the BIO-MAÏDO campaign is a unique opportunity to better understand the contribution of multiphase
665 atmospheric chemistry on SOA formation. However, deep analysis of the database does not allow to quantify this contribution even if it shows clear evidence of cloud processing on the OM composition of particles sampled at MO-5. Simulations with the explicit cloud chemistry model CLEPS is ongoing to investigate organic matter processing by cloud. A case study has been selected for this simulation, the 28th of March 2019 was chosen for several reasons: the amount of cloud water sampling was sufficient for allowing deep chemical composition analysis (Dominutti et al., 2022a), the observed cloud that day is typical of
670 a cloud forming on the slope at the end of the morning and evaporating before arriving at the MO-5 (see section 3.2), the operation of instruments was almost complete and there is evidence for sampling of air mass advected along the slope at MO-5 (Rocco et al., 2022). The CLEPS simulation is driven by meteorological, and cloud microphysical parameters extracted from a trajectory coming from the Meso-NH smallest domain (100m horizontal resolution) for this specific cloud event. The



675 contribution of biodegradation on the cloud processing will be assessed thanks to a recent development in the CLEPS model (Pailler et al., 2023). Biodegradation rates considered in the model have been determined using microbial strains that have been isolated from the puy de Dôme station. But this is not problematic since the comparison of the profiles of the phylum level distributions of bacteria isolates from clouds at Réunion Island and at puy de Dôme shows close similarities (Charpentier et al., submitted, 2022). Microorganisms' metabolic activities could be even more efficient at Réunion Island due to more elevated temperature, and this can be parametrized in the model.

680 In parallel with this 0d modeling, based on the 3D Meso-NH simulation made for the entire campaign, other Meso-NH simulations were made for the specific period from March 28 to 30. El Gdachi et al. (in prep), combined the size and composition of the observed aerosols to couple them to a two-moment microphysical scheme. This new detailed simulation also uses a very high vertical resolution (1m near the surface) to accurately represent anabatic and katabatic thermal circulations and the formation of clouds on the topography. Mouchel-Vallon et al. (in prep) carried out 3D studies combining gas-phase
685 chemistry and a detailed inventory of BVOC sources (100m) to study the modes of transport and oxidation of organic secondary aerosol precursors. Estimations of emissions of BVOC at HM-3 (see section 2.4) are used to calibrate and validate simulated emission fluxes. These both high-resolution 3D simulations (100m horizontal resolution and 1m vertical resolution near the surface) are able to correctly represent the life cycle of clouds and the main thermal circulations on slopes (anabatic and katabatic) as well as the source regions and isoprene oxidation mechanisms (El Gdachi et al, in prep; Mouchel-Vallon et
690 al., in prep). Finally, a specific simulation including gas-phase, aerosols and cloud chemistry with Meso-NH will be performed for the case studied with CLEPS. CLEPS simulation will help to select the dominant chemical pathways in aqueous phase to be considered and/or added in the Meso-NH chemical mechanism. 3D modelling allows considering complex effects of dynamics, deposition, emissions, and photochemistry on the air mass arriving at MO-5.

5. Conclusion

695 The BIO-MÄIDO campaign was dedicated to the observation of the effect of cloud on chemical composition of aerosols and especially the organic part in an environment dominated by natural and biogenic emissions. The Maïdo observatory, which was inaugurated at the end of 2012, was a unique opportunity to fulfil this objective because of its set of instrumentation (<https://www.osureunion.fr/les-stations-dobservation/opar/parametres-mesures/>, last access: 20 June 2023) and because of its geographical situation: tropical environment, quasi-daily cloud formation on the slope down the observatory for a specific part
700 of the year, isolated island with only reduced local anthropogenic influence, and endemic forest on the slope down the observatory. The strategy of the campaign and the choice of the deployed instrumentation was worked out to get the needed parameters to understand the chemical composition of aerosols sampled at the observatory and the signature of the cloud influence on it. The database from the campaign is original, combining dynamical, microphysical, chemical, biological, and particles' size parameters (droplets and aerosols).



705 The study of the mixing boundary layer air masses advected by thermal breezes at MO-5 during the daytime shows two preferred trajectories routes both corresponding to the return branches of the trade winds associated with the up-slopes thermal breezes. The first preferred route for air mass trajectories passed through the south allowing air masses to pass over the forests located between 1000 m and 1500 m asl in the south-west of the island. The route of the second set of trajectories is going up the western flank of the island, also indicating a passage in the marine boundary layer. A detailed analysis based on a high-
710 resolution Meso-NH simulation is made for the 28th of March. This analysis shows an important formation of clouds on the slope of the Maïdo at the end of the morning associated to the anabatic thermal breeze added with the trade winds return loop. These clouds evaporate before arriving at MO-5 indicating that aerosol particles measured at MO-5 can be thought to have undergone cloud processing during its transport on the slope.

The analysis of VOC measurements shows a highest mixing ratio of BTEX, isoprene and terpenes at PF-1. However, OVOC
715 is highest at HM-3 and the highest contributor of VOC mixing ratio at MO-5. The diminution of BTEX from PF-1 to HM-3 to MO-5 is a signature of the decrease of the influence of anthropogenic emissions along the slope to the Maïdo, as expected. The study of the chemical composition of particles at PF-1 and MO-5 during the daytime shows the presence of more oxidized organic aerosol at MO-5 and a higher concentration of oxalic acids at MO-5 than at PF-1. Both results indicate the presence of photochemical aged aerosols at MO-5, potentially impacted by cloud processing depending on the day and the trajectories
720 of air masses arriving at MO-5. The analysis of cloud chemical composition allows a thorough identification of organic compounds in cloud water. Despite this, around 80% in average of dissolved organic compounds in cloud water are undefined highlighting the complexity of the cloud organic matter.

These results, obtained from analysis of the BIO-MAÏDO campaign database, must be completed by numerical modeling to answer the three main objectives of the BIO-MAÏDO project i.e. understand which are the main formation pathways of SOA
725 in humid tropical atmosphere (gaseous phase versus aqueous phase); improve multiphase processes leading to SOA formation in a 3D model; examine whether the presence of bacteria in aqueous phase could contribute to SOA formation. To assess those objectives, simulations with the explicit cloud chemistry CLEPS model and the 3D Meso-NH are underway. Results from CLEPS will help to develop more complete chemical mechanisms for the 3D Meso-NH model to understand the role of biogenic influence on SOA formation in cloud water in tropical environment.

730 The BIO-MAÏDO project focuses on the effect of cloud on SOA formation in a tropical environment under biogenic influence dominated by isoprene emissions. During recent years, several studies using FT-ICR MS revealed that CHON formulas had high contribution to dissolved organic carbon in cloud water sampling in Colorado, USA (Zhao et al., 2013), NY, USA (Cook et al., 2027), the center of France (Bianco et al., 2018; 2019) and Southern China (Sun et al., 2021; Guo et al., 2023). Similar analysis is underway on three cloud samplings of the BIO-MAÏDO campaign. CHON compounds can have precursors from
735 biomass burning (BB), anthropogenic and biogenic emissions. For instance, Paglione et al. (2020) observed SOA formation by aqueous phase processing of wood combustion during wintertime in the Po Valley area under influence of fog and low-level clouds. Moreover, part of these compounds present in cloud water can lead to the formation of potentially toxic and harmful aqueous SOA as shown by Witkowski et al. (2022) in the lab, who studied the aqueous oxidation by OH of



nitrophenols. These recent developments in the analysis of the composition of cloud water and the formation of SOA through aqueous phase chemistry show a need to include more complete chemical mechanisms to understand the role of anthropogenic and BB influence on SOA formation in cloud/fog water, which is still not well understood. This can be investigated using available kinetics data and structure activity relationships for such chemical development (Hoffmann et al., 2018; Gonzales-Sanchez et al., 2021; Li et al., 2023). Future projects involving field campaigns following the BIO-MAÏDO methodology should be developed to assess a more complete understanding of the influence of cloud chemistry on the formation of AOS.

745 **Data availability**

The data from the BIO-MAÏDO campaign is freely available from <https://bio-maïdo.aeris-data.fr/catalogue/> (last access: 27 July 2023). The 3D simulations were produced with the Meso-NH code version 5.5.0 available at <http://mesonh.aero.obs-mip.fr/> (last access: 20 June 2023).

Author's contribution

750 ML is the principal investigator of the BIO-MAÏDO program, who designed the field campaign and prepared the manuscript with contributions from all the authors. PT organized the field campaign, produced, and organized the strategy for the Meso-NH simulations, and took part in the analysis of the results shown in the paper. LD led the Task 3 of the project on cloud sampling and characterization, wrote and reviewed the paper and took part of the field campaign. FB co-led the Task 1 dedicated to atmospheric dynamic and cloud properties, led the tethered balloon operations and the cloud microphysics instrumentation network. AC was responsible for the VOC measurements, wrote, and reviewed the paper related to gaseous atmospheric composition analysis and took part of the field experiments. AB co-led the Task 2 of the project related to the analysis of physico-chemical processes, wrote, and reviewed the paper related to gaseous atmospheric composition analysis and took part of the field experiments. CJ co-led the Task 2 of the project related to the analysis of physico-chemical processes, led the HM-3 station, participated to the field experiment and to the data treatment and analysis for this site. VD organized the field campaign and analyzed the lidar measurements. SH, JLJ and PD supervised the analyses of the off-line PM samples, processed these data, and commented the overall manuscript. MV co-organized and participated to the cloud droplets sampling and was responsible of the culture of bacteria from cloud samplings on site. PD supervised the analyses of the off-line PM samples and some of the analysis of cloud samples, processed these data, and commented the overall manuscript. MR wrote, and reviewed the paper related to gaseous atmospheric composition analysis and took part of the field experiments. CMV was involved the analysis of cloud chemistry measurements. SEG was involved in the dynamical analysis of the campaign. MB participated to the cloud sampling during the field campaign. MF and NM participated to the tethered balloon operations. BV operated the FLEXPART-AROME model, this included the design of the automated back-trajectory forecasting system which was operational during the BIO-MAÏDO campaign and providing updated footprints afterwards. CA, NS and BV were



770 responsible for the deployment, operation, and VOC database generation of the BIRA-IASB PTR-MS located at MO-5. VG
was responsible of the PTR-MS installed in the Atmo-Réunion truck and took part to the field campaign. JMP and MRi
participated to collect the cloud droplets and VOC and OVOC at PO-4. EP participated to the HM-3 station installation and to
the field experiment. EL participated to the field experiment and the HM-3 station disassembly. TB led in situ aerosol
measurements at DOS-2. AR, EM and JB participated to the tethered balloon operations. JMM was in charge of the technical
775 support at MO-5 for instrumentation deployed for the BIO-MÃIDO campaign. GP, CG, CB, JMT and AT were responsible
for the Atmo-Réunion truck deployment. EF, JLJ and PD wrote and reviewed the paper related to aerosols and clouds
composition analysis. KS was involved in the analysis of aerosol measurements. AMD was involved in the analysis of bacteria
measurements. PA and MJ isolated and identified microbial strains and performed metabarcoding sequencing. JLB performed
the back-trajectories and dynamical analysis. PR, Abi, LD and PD analyzed the cloud samples at the lab. AR was involved in
the dynamical analysis of the campaign. GP was involved in the lidar measurements and their analysis. All reviewed the paper.

780 Acknowledgments

The authors thank AERIS (French national pole for atmospheric services and data: <https://www.aeris-data.fr/>, last access: 20
June 2023) for his support on data storage. The French Meteorological Office (DIROI/Météo-France) also helped the
management of the campaign by providing a day-by-day meteorological forecasting. The authors gratefully acknowledge
CNRS-INSU (Institut National des Sciences de l'Univers) for supporting measurements performed at MO-5, which is part of
785 the SI-OPAR (Observatoire de Physique de l'Atmosphère à La Réunion), and those within the long-term monitoring aerosol
program SNO-CLAP (Climate relevant Aerosol Properties from near surface observations), both of which are components of
the ACTRIS French Research Infrastructure and whose data is hosted at the AERIS data center. The authors thank the staff of
UAR3365 in charge of reception at MO-5. Meso-NH simulations have been made on Météo-France supercomputer. Map data
used on Figure 1 are from OpenStreetMap (<https://www.openstreetmap.org/copyright/en>). Saint-Paul City Hall is thanked for
790 their support and their authorization to install scientific instrumentation on HM-3 site. All participants in the campaign wish
to thank Doudou for his hospitality on DOS-2 site.

Financial support

The BIO-MÃIDO project was funded by the Agence Nationale de la Recherche (ANR-18-CE01-0013). The deployment of
the BIRA-IASB PTR-MS at the Maïdo observatory was supported by the Belgian Federal Science Policy Office (grant no.
795 BR/175/A2/OCTAVE) with additional funding from Horizon 2020 (grant no. ACTRIS-2 (654109)).



References

- Amato, P., Joly, M., Besaury, L., Oudart, A., Taib, N., Moné, A. I., Deguillaume, L., Delort, A.-M., and Debroas, D.: Active microorganisms thrive among extremely diverse communities in cloud water, *PLOS ONE*, 12, e0182869, <https://doi.org/10.1371/journal.pone.0182869>, 2017.
- 800 Amelynck, C., Schoon, N., and Verreyken, B.: Long-term in situ (O) VOC measurements at the Maïdo observatory (Reunion Island) [Data Set], Royal Belgian Institute for Space Aeronomy (BIRA-IASB), <https://doi.org/10.18758/71021061>, 2021.
- Baray, J. L., Courcoux, Y., Keckhut, P., Portafaix, T., Tulet, P., Cammas, J. P., Hauchecorne, A., Godin Beekmann, S., De Mazière, M., Hermans, C., Desmet, F., Sellegri, K., Colomb, A., Ramonet, M., Sciare, J., Vuillemin, C., Hoareau, C., Dionisi, D., Dufлот, V., Vérèmes, H., Porteneuve, J., Gabarrot, F., Gaudo, T., Metzger, J. M., Payen, G., Leclair De Bellevue, J., Barthe, C., Posny, F., Ricaud, P., Abchiche, A. and Delmas, R.: Maïdo observatory: A new high-altitude station facility at Reunion Island (21 S, 55 E) for long-term atmospheric remote sensing and in situ measurements, *Atmos. Meas. Tech.*, 6(10), 2865–2877, <https://doi.org/10.5194/amt-6-2865-2013>, 2013.
- 805 Baray, J.-L., Deguillaume, L., Colomb, A., Sellegri, K., Freney, E., Rose, C., Van Baelen, J., Pichon, J.-M., Picard, D., Fréville, P., Bouvier, L., Ribeiro, M., Amato, P., Banson, S., Bianco, A., Borbon, A., Bourcier, L., Bras, Y., Brigante, M., Cacault, P., Chauvigné, A., Charbouillot, T., Chaumerliac, N., Delort, A.-M., Delmotte, M., Dupuy, R., Farah, A., Febvre, G., Flossmann, A., Gourbeyre, C., Hervier, C., Hervo, M., Huret, N., Joly, M., Kazan, V., Lopez, M., Mailhot, G., Marinoni, A., Masson, O., Montoux, N., Parazols, M., Peyrin, F., Pointin, Y., Ramonet, M., Rocco, M., Sancelme, M., Sauvage, S., Schmidt, M., Tison, E., Vaïtilingom, M., Villani, P., Wang, M., Yver-Kwok, C., and Laj, P.: Cézeaux-Aulnat-Opme-Puy De Dôme: a multi-site for the long-term survey of the tropospheric composition and climate change, *Atmos. Meas. Tech.*, 13, 3413–3445, <https://doi.org/10.5194/amt-13-3413-2020>, 2020.
- 815 Bauer, H., Schueller, E., Weinke, G., Berger, A., Hitzemberger, R., Marr, I. L., and Puxbaum, H.: Significant contributions of fungal spores to the organic carbon and to the aerosol mass balance of the urban atmospheric aerosol, *Atmos. Environ.*, 42, 5542–5549, <https://doi.org/10.1016/j.atmosenv.2008.03.019>, 2008.
- Benedict, K. B., Lee, T. and Collett, J. L.: Cloud water composition over the southeastern Pacific Ocean during the VOCALS regional experiment, *Atmos. Environ.*, 46, 104–114, <https://doi.org/10.1016/j.atmosenv.2011.10.029>, 2012.
- 820 Bianco, A., Vaïtilingom, M., Bridoux, M., Chaumerliac, N., Pichon, J.-M., Piro, J.-L. and Deguillaume, L.: Trace metals in cloud water sampled at the Puy de Dôme station, *Atmosphere*, 8(12), 225, <https://doi.org/10.3390/atmos8110225>, 2017.
- Bianco, A., Deguillaume, L., Vaïtilingom, M., Nicol, E., Baray, J. L., Chaumerliac, N., and Bridoux, M.: Molecular characterization of cloud water samples collected at the Puy de Dome (France) by Fourier Transform Ion Cyclotron Resonance Mass Spectrometry, *Environ. Sci. Technol.*, 52, 10275–10285, <https://doi.org/10.1021/acs.est.8b01964>, 2018.
- 825 Bianco, A., Riva, M., Baray, J.-L., Ribeiro, M., Chaumerliac, N., George, C., Bridoux, M., and Deguillaume, L.: Chemical characterization of cloudwater collected at Puy de Dôme by FT-ICR MS reveals the presence of SOA components, *ACS Earth Space Chem.*, 3, 2076–2087, <https://doi.org/10.1021/acsearthspacechem.9b00153>, 2019.



- 830 Borlaza, L. J. S., Weber, S., Uzu, G., Jacob, V., Cañete, T., Micallef, S., Trébuchon, C., Slama, R., Favez, O., and Jaffrezo, J.-
L.: Disparities in particulate matter (PM₁₀) origins and oxidative potential at a city scale (Grenoble, France) – Part 1: Source
apportionment at three neighbouring sites, *Atmos. Chem. Phys.*, 21, 5415–5437, <https://doi.org/10.5194/acp-21-5415-2021>,
2021.
- 835 Boucher, O., D. Randall, P. Artaxo, C. Bretherton, G. Feingold, P. Forster, V.-M. Kerminen, Y. Kondo, H. Liao, U. Lohmann,
P. Rasch, S.K. Satheesh, S. Sherwood, B. Stevens and X.Y. Zhang: Clouds and Aerosols. In: *Climate Change 2013: The
Physical Science Basis. Contribution of Working Group I to the Fifth Assessment Report of the Intergovernmental Panel on
Climate Change* [Stocker, T.F., D. Qin, G.-K. Plattner, M. Tignor, S.K. Allen, J. Boschung, A. Nauels, Y. Xia, V. Bex and
P.M. Midgley (eds.)]. Cambridge University Press, Cambridge, United Kingdom and New York, NY, USA, 2013.
- 840 Brito, J., Freney, E., Dominutti, P., Borbon, A., Haslett, S. L., Batenburg, A. M., Colomb, A., Dupuy, R., Denjean, C., Burnet,
F., Bourriane, T., Deroubaix, A., Sellegri, K., Borrmann, S., Coe, H., Flamant, C., Knippertz, P., and Schwarzenboeck, A.:
Assessing the role of anthropogenic and biogenic sources on PM₁ over southern West Africa using aircraft measurements,
Atmos. Chem. Phys., 18, 757–772, <https://doi.org/10.5194/acp-18-757-2018>, 2018.
- Canonaco, F., Crippa, M., Slowik, J. G., Baltensperger, U., and Prévôt, A. S. H.: SoFi, an IGOR-based interface for the efficient
use of the generalized multilinear engine (ME-2) for the source apportionment: ME-2 application to aerosol mass spectrometer
data, *Atmos. Meas. Tech.*, 6, 3649–3661, <https://doi.org/10.5194/amt-6-3649-2013>, 2013.
- 845 Caporaso, J. G., Lauber, C. L., Walters, W. A., Berg-Lyons, D., Huntley, J., Fierer, N., Owens, S. M., Betley, J., Fraser, L.,
Bauer, M., Gormley, N., Gilbert, J. A., Smith, G., and Knight, R.: Ultra-high-throughput microbial community analysis on the
Illumina HiSeq and MiSeq platforms, *ISME J.*, 6, 1621–1624, <https://doi.org/10.1038/ismej.2012.8>, 2012
- Carlton, A.G., B.J. Turpin, K.E. Altieri, S. Seitzinger, A. Reff, H.-J. Lim and B. Ervens: Atmospheric oxalic acid and SOA
production from glyoxal: Results of aqueous photooxidation experiments, *Atmos. Environ.*, 41, 7588-7602, 2007.
- 850 Cavalli, F., Viana, M., Yttri, K. E., Genberg, J., and Putaud, J.-P.: Toward a standardised thermal-optical protocol for
measuring atmospheric organic and elemental carbon: the EUSAAR protocol, *Atmos. Meas. Tech.*, 3, 79–89,
<https://doi.org/10.5194/amt-3-79-2010>, 2010.
- Cheng, C., Wang, G., Zhou, B., Meng, J., Li, J., Cao, J., and Xiao, S.: Comparison of dicarboxylic acids and related compounds
in aerosol samples collected in Xi'an, China during haze and clean periods, *Atmos. Environ.*, 81, 443–449,
855 <https://doi.org/10.1016/j.atmosenv.2013.09.013>, 2013.
- Cook, R. D., Lin, Y.-H., Peng, Z., Boone, E., Chu, R. K., Dukett, J. E., Gunsch, M. J., Zhang, W., Tolic, N., Laskin, A., and
Pratt, K. A.: Biogenic, urban, and wildfire influences on the molecular composition of dissolved organic compounds in cloud
water, *Atmos. Chem. Phys.*, 17, 15167–15180, <https://doi.org/10.5194/acp-17-15167-2017>, 2017.
- 860 Deguillaume, L., Charbouillot, T., Joly, M., Vaïtilingom, M., Parazols, M., Marinoni, A., Amato, P., Delort, A. M., Vinatier,
V., Flossmann, A., Chaumerliac, N., Pichon, J. M., Houdier, S., Laj, P., Sellegri, K., Colomb, A., Brigante, M. and Mailhot,
G.: Classification of clouds sampled at the puy de Dôme (France) based on 10 yr of monitoring of their physicochemical
properties, *Atmos. Chem. Phys.*, 14(3), 1485–1506, <https://doi.org/10.5194/acp-14-1485-2014>, 2014.



- Dominutti, P. A., Renard, P., Vaïtilingom, M., Bianco, A., Baray, J.-L., Borbon, A., Bourianne, T., Burnet, F., Colomb, A., Delort, A.-M., Dufлот, V., Houdier, S., Jaffrezo, J.-L., Joly, M., Lereboure, M., Metzger, J.-M., Pichon, J.-M., Ribeiro, M., Rocco, M., Tulet, P., Vella, A., Leriche, M., and Deguillaume, L.: Insights into tropical cloud chemistry at Reunion Island (Indian Ocean): results from the BIO-MAÏDO campaign, *Atmos. Chem. Phys.*, 22, 505–533, <https://doi.org/10.5194/acp-22-505-2022>, 2022a.
- Dominutti, P. A., Chevassus, E., Baray, J.-L., Jaffrezo, J.-L., Borbon, A., Colomb, A., Deguillaume, L., El Gdachi, S., Houdier, S., Leriche, M., Metzger, J.-M., Rocco, M., Tulet, P., Sellegri, K., and Freney, E.: Evaluation of sources, precursors, and processing of aerosols at a high-altitude tropical site, *ACS Earth Space Chem.*, 6, 2412–2431, <https://doi.org/10.1021/acsearthspacechem.2c00149>, 2022b.
- Dufлот, V., Tulet, P., Flores, O., Barthe, C., Colomb, A., Deguillaume, L., Vaïtilingom, M., Perring, A., Huffman, A., Hernandez, M. T., Sellegri, K., Robinson, E., O'Connor, D. J., Gomez, O. M., Burnet, F., Bourianne, T., Strasberg, D., Rocco, M., Bertram, A. K., Chazette, P., Totems, J., Fournel, J., Stamenoff, P., Metzger, J.-M., Chabasset, M., Rousseau, C., Bourianne, E., Sancelme, M., Delort, A.-M., Wegener, R. E., Chou, C., and Elizondo, P.: Preliminary results from the FARCE 2015 campaign: multidisciplinary study of the forest–gas–aerosol–cloud system on the tropical island of La Réunion, *Atmos. Chem. Phys.*, 19, 10591–10618, <https://doi.org/10.5194/acp-19-10591-2019>, 2019.
- Ervens, B., Turpin, B. J., and Weber, R. J.: Secondary organic aerosol formation in cloud droplets and aqueous particles (aqSOA): a review of laboratory, field and model studies, *Atmos. Chem. Phys.*, 11, 11069–11102, <https://doi.org/10.5194/acp-11-11069-2011>, 2011.
- Ervens, B., Turpin, B. J., and Weber, R. J.: Secondary organic aerosol formation in cloud droplets and aqueous particles (aqSOA): a review of laboratory, field and model studies, 11, 11069–11102, <https://doi.org/10.5194/acp-11-11069-2011>, 2011.
- Ervens, B.: Modeling the Processing of Aerosol and Trace Gases in Clouds and Fogs, *Chem. Rev.*, 115, 4157–4198, <https://doi.org/10.1021/cr5005887>, 2015.
- Ervens, B. and Amato, P.: The global impact of bacterial processes on carbon mass, *Atmos. Chem. Phys.*, 20, 1777–1794, <https://doi.org/10.5194/acp-20-1777-2020>, 2020.
- Escudié, F., Auer, L., Bernard, M., Mariadassou, M., Cauquil, L., Vidal, K., Maman, S., Hernandez-Raquet, G., Combes, S., and Pascal, G.: FROGS: Find, Rapidly, OTUs with Galaxy Solution, *Bioinformatics*, 34, 1287–1294, <https://doi.org/10.1093/bioinformatics/btx791>, 2018.
- Fathalli M., Lac, C., Burnet, F., and Vié, B.: Formation of fog due to stratus lowering: an observational and modelling case study, *Quart. J. Roy. Meteor. Soc.*, 148, 2299 - 2324. <https://doi.org/10.1002/qj.4304>, 2022.
- Fomba, K. W., Müller, K., van Pinxteren, D. and Herrmann, H.: Aerosol size-resolved trace metal composition in remote northern tropical Atlantic marine environment: Case study cape verde islands, *Atmos. Chem. Phys.*, 13(9), 4801–4814, <https://doi.org/10.5194/acp-13-4801-2013>, 2013.



- 895 Fomba, K. W., Deabji, N., Barcha, S. E. I., Ouchen, I., Elbaramoussi, E. M., El Moursli, R. C., Harnafi, M., El Hajjaji, S., Mellouki, A. and Herrmann, H.: Application of TXRF in monitoring trace metals in particulate matter and cloud water, *Atmos. Meas. Tech.*, 13(9), 4773–4790, doi:10.5194/amt-13-4773-2020, 2020.
- Gioda, A., Mayol-Bracero, O. L., Scatena, F. N., Weathers, K. C., Mateus, V. L. and McDowell, W. H.: Chemical constituents in clouds and rainwater in the Puerto Rican rainforest: Potential sources and seasonal drivers, *Atmos. Environ.*, 68, 208–220, 900 <https://doi.org/10.1016/j.atmosenv.2012.11.017>, 2013
- Foucart, B., Sellegri, K., Tulet, P., Rose, C., and Metzger, J.-M., and Picard, D.: High occurrence of new particle formation events at the Maïdo high-altitude observatory (2150 m), Réunion (Indian Ocean). *Atmos. Chem. Phys.*, 2018, 18, 9243–9261, <https://doi.org/10.5194/acp-18-9243-2018>, 2018.
- Golly, B., Waked, A., Weber, S., Samake, A., Jacob, V., Conil, S., Rangognio, J., Chrétien, E., Vagnot, M.-P., Robic, P.-Y., 905 Besombes, J.-L., and Jaffrezo, J.-L.: Organic markers and OC source apportionment for seasonal variations of PM_{2.5} at 5 rural sites in France, *Atmos. Environ.*, 198, 142–157, <https://doi.org/10.1016/j.atmosenv.2018.10.027>, 2019.
- González-Sánchez, J. M., Brun, N., Wu, J., Morin, J., Temime-Roussel, B., Ravier, S., Mouchel-Vallon, C., Clément, J.-L., and Monod, A.: On the importance of atmospheric loss of organic nitrates by aqueous-phase ·OH oxidation, *Atmos. Chem. Phys.*, 21, 4915–4937, <https://doi.org/10.5194/acp-21-4915-2021>, 2021.
- 910 Guenther, A. B., Zimmerman, P. R., Harley, P. C., Monson, R. K., and Fall, R.: Isoprene and Monoterpene Emission Rate Variability – Model Evaluations and Sensitivity Analyses, *J. Geophys. Res. Atmos.*, 98, 12 609–12 617, 1993
- Guenther, A. B., Jiang, X., Heald, C. L., Sakulyanontvittaya, T., Duhl, T., Emmons, L. K., and Wang, X.: The Model of Emissions of Gases and Aerosols from Nature version 2.1 (MEGAN2.1): an extended and updated framework for modeling biogenic emissions, *Geosci. Model Dev.*, 5, 1471–1492, <https://doi.org/10.5194/gmd-5-1471-2012>, 2012.
- 915 Guilpart, E., Vimeux, F., Evan, S., Brioude, J., Metzger, J.-M., Barthe, C., Risi, C., and Cattani, O.: The isotopic composition of near-surface water vapor at the Maïdo observatory (Reunion Island, southwestern Indian Ocean) documents the controls of the humidity of the subtropical troposphere, *J. Geophys. Res. Atmos.*, 122, 9628–9650, <https://doi.org/10.1002/2017JD026791>, 2017.
- Guo, Z., Sun, W., Hu, X., Lin, J., Fu, Y., Peng, X., Jiang, B., Liao, Y., Zhang, G., Wang, X., Peng, P., and Bi, X.: Molecular 920 characteristics and compositions affecting light absorption features of cloud water revealed by Fourier transform ion cyclotron resonance mass spectrometry, *Atmos. Environ.*, 295, 119565, <https://doi.org/10.1016/j.atmosenv.2022.119565>, 2023.
- Heald, C. L., Coe, H., Jimenez, J. L., Weber, R. J., Bahreini, R., Middlebrook, A. M., Russell, L. M., Jolleys, M., Fu, T.-M., Allan, J. D., Bower, K. N., Capes, G., Crosier, J., Morgan, W. T., Robinson, N. H., Williams, P. I., Cubison, M. J., DeCarlo, P. F., and Dunlea, E. J.: Exploring the vertical profile of atmospheric organic aerosol: comparing 17 aircraft field campaigns 925 with a global model, *Atmos. Chem. Phys.*, 11, 12673–12696, <https://doi.org/10.5194/acp-11-12673-2011>, 2011.
- Jaffrezo, J.-L., Aymoz, G., Delaval, C., and Cozic, J.: Seasonal variations of the water soluble organic carbon mass fraction of aerosol in two valleys of the French Alps, *Atmos. Chem. Phys.*, 5, 2809–2821, <https://doi.org/10.5194/acp-5-2809-2005>, 2005.



- Jathar, S. H., Cappa, C. D., Wexler, A. S., Seinfeld, J. H., and Kleeman, M. J.: Simulating secondary organic aerosol in a regional air quality model using the statistical oxidation model – Part 1: Assessing the influence of constrained multi-
930 generational ageing, *Atmos. Chem. Phys.*, 16, 2309–2322, <https://doi.org/10.5194/acp-16-2309-2016>, 2016.
- Jimenez, J. L., Canagaratna, M. R., Donahue, N. M., Prevot, A. S. H., Zhang, Q., Kroll, J. H., DeCarlo, P. F., Allan, J. D., Coe, H., Ng, N. L., Aiken, A. C., Docherty, K. S., Ulbrich, I. M., Grieshop, A. P., Robinson, A. L., Duplissy, J., Smith, J. D., Wilson, K. R., Lanz, V. A., Hueglin, C., Sun, Y. L., Tian, J., Laaksonen, A., Raatikainen, T., Rautiainen, J., Vaattovaara, P., Ehn, M., Kulmala, M., Tomlinson, J. M., Collins, D. R., Cubison, M. J., E., Dunlea, J., Huffman, J. A., Onasch, T. B., Alfarra,
935 M. R., Williams, P. I., Bower, K., Kondo, Y., Schneider, J., Drewnick, F., Borrmann, S., Weimer, S., Demerjian, K., Salcedo, D., Cottrell, L., Griffin, R., Takami, A., Miyoshi, T., Hatakeyama, S., Shimono, A., Sun, J. Y., Zhang, Y. M., Dzepina, K., Kimmel, J. R., Sueper, D., Jayne, J. T., Herndon, S. C., Trimborn, A. M., Williams, L. R., Wood, E. C., Middlebrook, A. M., Kolb, C. E., Baltensperger, U., and Worsnop, D. R.: Evolution of Organic Aerosols in the Atmosphere, *Science*, 326, 1525–1529, <https://doi.org/10.1126/science.1180353>, 2009.
- 940 Kawamura, K. and Sakaguchi, F.: Molecular distributions of water soluble dicarboxylic acids in marine aerosols over the Pacific Ocean including tropics, *J. Geophys. Res. Atmos.*, 104, 3501–3509, <https://doi.org/10.1029/1998JD100041>, 1999.
- Kawamura, K. and Bikkina, S.: A review of dicarboxylic acids and related compounds in atmospheric aerosols: Molecular distributions, sources and transformation, *Atmos. Res.*, 170, 140–160, <https://doi.org/10.1016/j.atmosres.2015.11.018>, 2016.
- Khaled, A., Zhang, M., Amato, P., Delort, A.-M., and Ervens, B.: Biodegradation by bacteria in clouds: an underestimated
945 sink for some organics in the atmospheric multiphase system, *Atmos. Chem. Phys.*, 21, 3123–3141, <https://doi.org/10.5194/acp-21-3123-2021>, 2021.
- Lac, C., Chaboureau, J.-P., Masson, V., Pinty, J.-P., Tulet, P., Escobar, J., Leriche, M., Barthe, C., Aouizerats, B., Augros, C., Aumond, P., Auguste, F., Bechtold, P., Berthet, S., Bielli, S., Bosseur, F., Caumont, O., Cohard, J.-M., Colin, J., Couvreux, F., Cuxart, J., Delautier, G., Dauhut, T., Ducrocq, V., Filippi, J.-B., Gazen, D., Geoffroy, O., Gheusi, F., Honnert, R., Lafore,
950 J.-P., Lebeaupin Brossier, C., Libois, Q., Lunet, T., Mari, C., Maric, T., Mascart, P., Mogé, M., Molinié, G., Nuissier, O., Pantillon, F., Peyrillé, P., Pergaud, J., Perraud, E., Pianezze, J., Redelsperger, J.-L., Ricard, D., Richard, E., Riette, S., Rodier, Q., Schoetter, R., Seyfried, L., Stein, J., Suhre, K., Taufour, M., Thouron, O., Turner, S., Verrelle, A., Vié, B., Visentin, F., Vionnet, V., and Wautelet, P.: Overview of the Meso-NH model version 5.4 and its applications, *Geosci. Model Dev.*, 11, 1929–1969, <https://doi.org/10.5194/gmd-11-1929-2018>, 2018.
- 955 Lesouëf, D., Gheusi, F., Delmas, R. and Escobar, J.: Numerical simulations of local circulations and pollution transport over Reunion Island, *Ann. Geophys.*, 29(1), 53–69, <https://doi.org/10.5194/angeo-29-53-2011>, 2011.
- Lesouëf, D., Gheusi, F., Chazette, P., Delmas, R. and Sanak, J.: Low Tropospheric Layers Over Reunion Island in Lidar-Derived Observations and a High-Resolution Model, *Boundary-Layer Meteorol.*, 149(3), 425–453, <https://doi.org/10.1007/s10546-013-9851-9>, 2013.
- 960 Li, F., Zhou, S., Du, L., Zhao, J., Hang, J., and Wang, X.: Aqueous-phase chemistry of atmospheric phenolic compounds: A critical review of laboratory studies, *Sci. Total Environ.*, 856, 158895, <https://doi.org/10.1016/j.scitotenv.2022.158895>, 2023.



- Liu, Y., I. El Haddad, M. Scarfogliero, L. Nieto-Gligorovski, B. Temime-Roussel, E. Quivet, N. Marchand, B. Picquet-Varrault, and A. Monod: In-cloud processes of methacrolein under simulated conditions ? Part 1: Aqueous phase photooxidation, *Atmos. Chem. Phys.*, 9, 5093–5105, 2009.
- 965 Molina, L., Wittich, R.-M., van Dillewijn, P., and Segura, A.: Plant-Bacteria Interactions for the Elimination of Atmospheric Contaminants in Cities, *Agronomy*, 11, 493, <https://doi.org/10.3390/agronomy11030493>, 2021.
- Mouchel-Vallon, C., Deguillaume, L., Monod, A., Perroux, H., Rose, C., Ghigo, G., Long, Y., Leriche, M., Aumont, B., Patryl, L., Armand, P., and Chaumerliac, N.: CLEPS 1.0: A new protocol for cloud aqueous phase oxidation of VOC mechanisms, *Geosci. Model Dev.*, 10, 1339–1362, <https://doi.org/10.5194/gmd-10-1339-2017>, 2017.
- 970 Paglione, M., Gilardoni, S., Rinaldi, M., Decesari, S., Zanca, N., Sandrini, S., Giulianelli, L., Bacco, D., Ferrari, S., Poluzzi, V., Scotto, F., Trentini, A., Poulain, L., Herrmann, H., Wiedensohler, A., Canonaco, F., Prévôt, A. S. H., Massoli, P., Carbone, C., Facchini, M. C., and Fuzzi, S.: The impact of biomass burning and aqueous-phase processing on air quality: a multi-year source apportionment study in the Po Valley, Italy, *Atmos. Chem. Phys.*, 20, 1233–1254, <https://doi.org/10.5194/acp-20-1233-2020>, 2020.
- 975 Pai, S. J., Heald, C. L., Pierce, J. R., Farina, S. C., Marais, E. A., Jimenez, J. L., Campuzano-Jost, P., Nault, B. A., Middlebrook, A. M., Coe, H., Shilling, J. E., Bahreini, R., Dingle, J. H., and Vu, K.: An evaluation of global organic aerosol schemes using airborne observations, *Atmos. Chem. Phys.*, 20, 2637–2665, <https://doi.org/10.5194/acp-20-2637-2020>, 2020.
- Pailler, L., Wirgot, N., Joly, M., Renard, P., Mouchel-Vallon, C., Bianco, A., Leriche, M., Sancelme, M., Job, A., Patryl, L., Armand, P., Delort, A.-M., Chaumerliac, N., and Deguillaume, L.: Assessing the efficiency of water-soluble organic compound biodegradation in clouds under various environmental conditions, *Environ. Sci.: Atmos.*, 3, 731–748, <https://doi.org/10.1039/D2EA00153E>, 2023.
- Péguilhan, R., Besaury, L., Rossi, F., Enault, F., Baray, J.-L., Deguillaume, L., and Amato, P.: Rainfalls sprinkle cloud bacterial diversity while scavenging biomass, *FEMS Microbiology Ecology*, 97, <https://doi.org/10.1093/femsec/fiab144>, 2021.
- Pisso, I., Sollum, E., Grythe, H., Kristiansen, N. I., Cassiani, M., Eckhardt, S., Arnold, D., Morton, D., Thompson, R. L., Groot
- 985 Zwaafink, C. D., Evangeliou, N., Sodemann, H., Haimberger, L., Henne, S., Brunner, D., Burkhardt, J. F., Fouilloux, A., Brioude, J., Philipp, A., Seibert, P., and Stohl, A.: The Lagrangian particle dispersion model FLEXPART version 10.4, *Geosci. Model Dev.* 12, 4955–4997, <https://doi.org/10.5194/gmd-12-4955-2019>, 2019.
- Quast, C., Pruesse, E., Yilmaz, P., Gerken, J., Schweer, T., Yarza, P., Peplies, J., and Glöckner, F. O.: The SILVA ribosomal RNA gene database project: improved data processing and web-based tools, *Nucleic Acids Res*, 41, D590–D596, <https://doi.org/10.1093/nar/gks1219>, 2013.
- 990 Réchou, A., Flores, O., Jumaux, G., DufLOT, V., Bousquet, O., Pouppeville, C., and Bonnardot, F.: Spatio-temporal variability of rainfall in a high tropical island: Patterns and large-scale drivers in Réunion Island, *Quarterly J. Royal Meteor. Soc.*, 145, 893–909, <https://doi.org/10.1002/qj.3485>, 2019.



- Renard, P., Siekmann, F., Salque, G., Demelas, C., Coulomb, B., Vassalo, L., Ravier, S., Temime-Roussel, B., Voisin, D., and
995 Monod, A.: Aqueous-phase oligomerization of methyl vinyl ketone through photooxidation – Part 1: Aging processes of
oligomers, *Atmos. Chem. Phys.*, 15, 21–35, <https://doi.org/10.5194/acp-15-21-2015>, 2015.
- Renard, P., Brissy, M., Rossi, F., Lereboure, M., Jaber, S., Baray, J.-L., Bianco, A., Delort, A.-M., and Deguillaume, L.:
Free amino acid quantification in cloud water at the Puy de Dôme station (France), *Atmos. Chem. Phys.*, 22, 2467–2486,
<https://doi.org/10.5194/acp-22-2467-2022>, 2022.
- 1000 Reyes-Rodríguez, G. J., Gioda, A., Mayol-Bracero, O. L. and Collett, J.: Organic carbon, total nitrogen, and water-soluble
ions in clouds from a tropical montane cloud forest in Puerto Rico, *Atmos. Environ.*, 43(27), 4171–4177,
<https://doi.org/10.1016/j.atmosenv.2009.05.049>, 2009.
- Rocco, M., Colomb, A., Baray, J. L., Amelynck, C., Verreyken, B., Borbon, A., Pichon, J. M., Bouvier, L., Schoon, N., Gros,
V., Sarda-Esteve, R., Tulet, P., Metzger, J. M., Dufлот, V., Guadagno, C., Peris, G. and Brioude, J.: Analysis of volatile organic
1005 compounds during the OCTAVE campaign: Sources and distributions of formaldehyde on reunion Island, *Atmosphere*, 11(2),
<https://doi.org/10.3390/atmos11020140>, 2020.
- Rocco, M., Baray, J.-L., Colomb, A., Borbon, A., Dominutti, P., Tulet, P., Amelynck, C., Schoon, N., Verreyken, B., Dufлот,
V., Gros, V., Sarda-Estève, R., Péris, G., Guadagno, C., and Leriche, M.: High resolution dynamical analysis of Volatile
Organic Compounds (VOC) measurements during the BIO-MAÏDO field campaign (Réunion Island, Indian Ocean), *J.*
1010 *Geophys. Res. Atmos.*, 127, e2021JD035570, <https://doi.org/10.1029/2021JD035570>, 2022.
- Rose, C., Chaumerliac, N., Deguillaume, L., Perroux, H., Mouchel-Vallon, C., Leriche, M., Patryl, L., and Armand, P.:
Modeling the partitioning of organic chemical species in cloud phases with CLEPS (1.1), *Atmos. Chem. Phys.*, 18, 2225–
2242, <https://doi.org/10.5194/acp-18-2225-2018>, 2018.
- Rose, C., Foucart, B., Picard, D., Colomb, A., Metzger, J.-M., Tulet, P., and Sellegri, K.: New particle formation in the volcanic
1015 eruption plume of the Piton de la Fournaise: specific features from a long-term dataset, *Atmos. Chem. Phys.*, 19, 13243–13265,
<https://doi.org/10.5194/acp-19-13243-2019>, 2019.
- Samaké, A., Jaffrezo, J.-L., Favez, O., Weber, S., Jacob, V., Albinet, A., Riffault, V., Perdrix, E., Waked, A., Golly, B.,
Salameh, D., Chevrier, F., Oliveira, D. M., Bonnaire, N., Besombes, J.-L., Martins, J. M. F., Conil, S., Guillaud, G., Mesbah,
B., Rocq, B., Robic, P.-Y., Hulin, A., Meur, S. L., Descheemaeker, M., Chretien, E., Marchand, N., and Uzu, G.: Polyols and
1020 glucose particulate species as tracers of primary biogenic organic aerosols at 28 French sites, *Atmos. Chem. Phys.*, 19, 3357–
3374, <https://doi.org/10.5194/acp-19-3357-2019>, 2019.
- Shrivastava, M., Cappa, C. D., Fan, J., Goldstein, A. H., Guenther, A. B., Jimenez, J. L., Kuang, C., Laskin, A., Martin, S. T.,
Ng, N. L., Petaja, T., Pierce, J. R., Rasch, P. J., Roldin, P., Seinfeld, J. H., Shilling, J., Smith, J. N., Thornton, J. A., Volkamer,
R., Wang, J., Worsnop, D. R., Zaveri, R. A., Zelenyuk, A., and Zhang, Q.: Recent advances in understanding secondary organic
1025 aerosol: Implications for global climate forcing, *Rev. Geophys.*, 2016RG000540, <https://doi.org/10.1002/2016RG000540>,
2017.



- Simoneit, B. R. T.: Biomass burning — a review of organic tracers for smoke from incomplete combustion, *Applied Geochem.*, 17, 129–162, [https://doi.org/10.1016/S0883-2927\(01\)00061-0](https://doi.org/10.1016/S0883-2927(01)00061-0), 2002.
- Simu, S. A., Miyazaki, Y., Tachibana, E., Finkenzeller, H., Brioude, J., Colomb, A., Magand, O., Verreyken, B., Evan, S.,
1030 Volkamer, R., and Stavrou, T.: Origin of water-soluble organic aerosols at the Maïdo high-altitude observatory, Réunion Island, in the tropical Indian Ocean, *Atmos. Chem. Phys.*, 21, 17017–17029, <https://doi.org/10.5194/acp-21-17017-2021>, 2021.
- Stahl, C., Crosbie, E., Bañaga, P. A., Betito, G., Braun, R. A., Cainglet, Z. M., Cambaliza, M. O., Cruz, M. T., Dado, J. M., Hilario, M. R. A., Leung, G. F., MacDonald, A. B., Magnaye, A. M., Reid, J., Robinson, C., Shook, M. A., Simpas, J. B.,
1035 Visaga, S. M., Winstead, E., Ziemba, L., and Sorooshian, A.: Total organic carbon and the contribution from speciated organics in cloud water: airborne data analysis from the CAMP2Ex field campaign, *Atmos. Chem. Phys.*, 21, 14109–14129, <https://doi.org/10.5194/acp-21-14109-2021>, 2021.
- Su, H., Cheng, Y., and Pöschl, U.: New Multiphase Chemical Processes Influencing Atmospheric Aerosols, Air Quality, and Climate in the Anthropocene, *Acc. Chem. Res.*, 53, 2034–2043, <https://doi.org/10.1021/acs.accounts.0c00246>, 2020.
- 1040 Sun, W., Fu, Y., Zhang, G., Yang, Y., Jiang, F., Lian, X., Jiang, B., Liao, Y., Bi, X., Chen, D., Chen, J., Wang, X., Ou, J., Peng, P., and Sheng, G.: Measurement report: Molecular characteristics of cloud water in southern China and insights into aqueous-phase processes from Fourier transform ion cyclotron resonance mass spectrometry, *Atmos. Chem. Phys.*, 21, 16631–16644, <https://doi.org/10.5194/acp-21-16631-2021>, 2021.
- Triesch, N., van Pinxteren, M., Engel, A. and Herrmann, H.: Concerted measurements of free amino acids at the Cabo Verde islands: high enrichments in submicron sea spray aerosol particles and cloud droplets, *Atmos. Chem. Phys.*, 21(1), 163–181, <https://doi.org/10.5194/acp-21-163-2021>, 2021.
- 1045 Tsui, W. G., Woo, J. L., and McNeill, V. F.: Impact of aerosol-cloud cycling on aqueous secondary organic aerosol formation, *Atmosphere*, 10, 666, <https://doi.org/10.3390/atmos10110666>, 2019.
- Vaïtilingom, M., Attard, E., Gaiani, N., Sancelme, M., Deguillaume, L., Flossmann, A. I., Amato, P., and Delort, A.-M.: Long-term features of cloud microbiology at the puy de Dôme (France), *Atmos. Environ.*, 56, 88–100, <https://doi.org/10.1016/j.atmosenv.2012.03.072>, 2012.
- 1050 Van Pinxteren, D., Plewka, A., Hofmann, D., Müller, K., Kramberger, H., Svrčina, B., Bächmann, K., Jaeschke, W., Mertes, S., Collett, J. L., and Herrmann, H.: Schmücke hill cap cloud and valley stations aerosol characterisation during FEBUKO (II): Organic compounds, *Atmos. Environ.*, 39, 4305–4320, <https://doi.org/10.1016/j.atmosenv.2005.02.014>, 2005.
- 1055 Verma, S. K., Kawamura, K., Chen, J. and Fu, P.: Thirteen years of observations on primary sugars and sugar alcohols over remote Chichijima Island in the western North Pacific, *Atmos. Chem. Phys.*, 18(1), 81–101, <https://doi.org/10.5194/acp-18-81-2018>, 2018.
- Verreyken, B., Brioude, J., and Evan, S.: Development of turbulent scheme in the FLEXPART-AROME v1.2.1 Lagrangian particle dispersion model, *Geosci. Model Dev.*, 12, 4245–4259, <https://doi.org/10.5194/gmd-12-4245-2019>, 2019.



- 1060 Verreyken, B., Amelynck, C., Brioude, J., Müller, J.-F., Schoon, N., Kumps, N., Colomb, A., Metzger, J.-M., Lee, C. F.,
Koenig, T. K., Volkamer, R., and Stavrakou, T.: Characterisation of African biomass burning plumes and impacts on the
atmospheric composition over the south-west Indian Ocean, *Atmos. Chem. Phys.*, 20, 14821–14845,
<https://doi.org/10.5194/acp-20-14821-2020>, 2020.
- Verreyken, B., Amelynck, C., Schoon, N., Müller, J.-F., Brioude, J., Kumps, N., Hermans, C., Metzger, J.-M., Colomb, A.,
1065 and Stavrakou, T.: Measurement report: Source apportionment of volatile organic compounds at the remote high-altitude
Maïdo observatory, *Atmos. Chem. Phys.*, 21, 12965–12988, <https://doi.org/10.5194/acp-21-12965-2021>, 2021.
- Wang, H., Kawamura, K., and Yamazaki, K.: Water-Soluble dicarboxylic acids, ketoacids and dicarbonyls in the atmospheric
aerosols over the southern ocean and western pacific ocean, *J. Atmos. Chem.*, 53, 43–61, <https://doi.org/10.1007/s10874-006-1479-4>, 2006.
- 1070 Wang, M., Perroux, H., Fleuret, J., Bianco, A., Bouvier, L., Colomb, A., Borbon, A., and Deguillaume, L.: Anthropogenic and
biogenic hydrophobic VOCs detected in clouds at the puy de Dôme station using Stir Bar Sorptive Extraction: Deviation from
the Henry's law prediction, *Atmos. Res.*, 237, 104844, <https://doi.org/10.1016/j.atmosres.2020.104844>, 2020.
- Witkowski, B., Jain, P., and Gierczak, T.: Aqueous chemical bleaching of 4-nitrophenol brown carbon by hydroxyl radicals;
products, mechanism, and light absorption, *Atmos. Chem. Phys.*, 22, 5651–5663, <https://doi.org/10.5194/acp-22-5651-2022>,
1075 2022.
- World Health Organization – Regional Office for Europe: Review of evidence on health aspects of air pollution: REVIHAAP
project: technical report, World Health Organization, Regional Office for Europe,
<https://apps.who.int/iris/handle/10665/341712>, 2021.
- Zhang, Q., et al.: Ubiquity and dominance of oxygenated species in organic aerosols in anthropogenically-influenced Northern
1080 Hemisphere midlatitudes, *Geophys. Res. Lett.*, 34, L13801, <https://doi.org/10.1029/2007gl029979>, 2007.
- Zhang, T., Engling, G., Chan, C.-Y., Zhang, Y.-N., Zhang, Z.-S., Lin, M., Sang, X.-F., Li, Y. D., and Li, Y.-S.: Contribution
of fungal spores to particulate matter in a tropical rainforest, *Environ. Res. Lett.*, 5, 024010, <https://doi.org/10.1088/1748-9326/5/2/024010>, 2010.
- Zhao, Y., Hallar, A. G., and Mazzoleni, L. R.: Atmospheric organic matter in clouds: exact masses and molecular formula
1085 identification using ultrahigh-resolution FT-ICR mass spectrometry, *Atmos. Chem. Phys.*, 13, 12343–12362,
<https://doi.org/10.5194/acp-13-12343-2013>, 2013.
- Zhu, C., Kawamura, K., and Kunwar, B.: Organic tracers of primary biological aerosol particles at subtropical Okinawa Island
in the western North Pacific Rim: organic biomarkers in the north pacific, *J. Geophys. Res. Atmos.*, 120, 5504–5523, 2015.